

Structural changes and picosecond to second dynamics of cytochrome c in interaction with nitric oxide in ferrous and ferric redox states

Sergei Kruglik, Byung-Kuk Yoo, Jean-Christophe Lambry, Jean-Louis Martin, Michel Negrerie

▶ **To cite this version:**

Sergei Kruglik, Byung-Kuk Yoo, Jean-Christophe Lambry, Jean-Louis Martin, Michel Negrerie. Structural changes and picosecond to second dynamics of cytochrome c in interaction with nitric oxide in ferrous and ferric redox states. Physical Chemistry Chemical Physics, 2017, 19 (32), pp.21317-21334. 10.1039/C7CP02634J . hal-01598497

HAL Id: hal-01598497

https://hal.sorbonne-universite.fr/hal-01598497

Submitted on 29 Sep 2017

HAL is a multi-disciplinary open access archive for the deposit and dissemination of scientific research documents, whether they are published or not. The documents may come from teaching and research institutions in France or abroad, or from public or private research centers.

L'archive ouverte pluridisciplinaire **HAL**, est destinée au dépôt et à la diffusion de documents scientifiques de niveau recherche, publiés ou non, émanant des établissements d'enseignement et de recherche français ou étrangers, des laboratoires publics ou privés.

Structural changes and picosecond to second dynamics of cytochrome *c* in interaction with nitric oxide in ferrous and ferric redox states

Sergei G. Kruglik[a,*], Byung-Kuk Yoo[b], Jean-Christophe Lambry[b], Jean-Louis Martin[b] and Michel Negrerie[b,*]

[a]*Laboratoire Jean Perrin, Sorbonne Universités, UPMC Univ. Paris 06, CNRS, 75005 Paris, France. E-mail*: sergei.kruglik@upmc.fr

[b]*Laboratoire d'Optique et Biosciences, INSERM, Ecole Polytechnique, 91128 Palaiseau, France. E-mail*: michel.negrerie@polytechnique.fr

Electronic supplementary information.

Apart a role in electron transfer, mitochondrial cytochrome *c* acts in apoptosis and is subject to nitrosylation. The cleavage of the Fe–Met80 bond plays a role in several processes including release of Cyt *c* from mitochondria or increase of its peroxydase activity. Nitrosylation of Cyt *c* precludes the reformation of disrupted Fe–Met80 bond and was shown to occur during apoptosis. These physiological properties are associated with a conformational change of the heme center of Cyt *c*. Here, we demonstrate that NO binding induces pronounced heme conformational changes in the six-coordinate Cyt *c*–NO complex. Equilibrium and time-resolved Raman data reveal that the heme structural conformation depends on both the nature of the distal iron ligand (NO or Met80) and on the Fe^{2+} or Fe^{3+} heme redox state. Upon nitrosylation, the heme ruffling distortion is greatly enhanced for ferrous Cyt *c*. Contrastingly, the initial strong heme distortion in native ferric Cyt *c* almost disappears after NO binding. We measured the heme coordination dynamics in picosecond to second time range and identified Met80 and NO rebinding phases by time-resolved Raman and absorption spectroscopies. Dissociation of NO instantly produces 5-coordinate heme with domed structure which continues to rearrange within 15 ps, while the initial ruffling distortion disappears. The rates of Cyt *c*–NO complex formation measured by transient absorption are $k_{on} = 1.81 \times 10^6$ $M^{-1}{\cdot}s^{-1}$ for ferric and 83 $M^{-1}{\cdot}s^{-1}$ for ferrous Cyt *c*. After NO dissociation and exit from the heme pocket, the rebinding of Met80 to the heme iron takes place 6 orders of magnitude slower (3 – 5 μs) than Met80 rebinding in the absence of NO (5 ps). Altogether, these data reveal structural and dynamic properties of Cyt *c* in interaction with nitric oxide relevant for molecular mechanism of apoptosis.

Introduction

Mitochondrial cytochrome *c* (Cyt *c*) acts as an universal electron carrier associated with an oxidase in mitochondria for the energetic process leading to ATP synthesis[1], but this small heme protein possesses also other functions[2]. In particular, it is involved in the mitochondrial apoptosis pathway initiated by the transmembrane FAS receptor activation.[3,4] Following caspases activation, the BAK protein triggers the release of Cyt *c* from mitochondria to cytoplasm through the outer mitochondrion membrane permeabilization.[2] Then Cyt *c* binds to Apaf-1 (Apoptotis protease activating factor) to form the functional apoptosome complex with caspase-9.[2,5] Within this apoptotic cascade, many structural mechanisms remain unknown at molecular level. It has been demonstrated that Cyt *c* released from mitochondria during apoptosis is nitrosylated,[6] the only case of nitric oxide (NO) binding to Cyt *c* in cell. Indeed, the activation of mitochondrial NO-synthase (NOS) triggers the release of Cyt *c* from mitochondria,[7] wheareas its inhibition of NOS by L-NMA induces an inhibition of apoptosis but the addition of exogenous nitrosylated Cyt *c* increases caspase activation.[6] This signaling event in the apoptotic pathway may be linked to the presence of NO-synthase in mitochondria.[8,9] Thus, the diatomic ligand binding property of the heme is also involved in cell death, besides its redox properties involved in its ubiquitous role in electron transfer. NO appears as a messenger which activates apoptosis through its binding to Cyt *c*, in contrast to its role in inhibiting apoptosis through different signaling pathways.[10,11,12]

The nitrosylation of Cyt *c* during apoptosis leads to the hypothesis that protein's structural changes, induced by the replacement of Met80 with NO bound to the heme, promote Cyt *c* binding to Apaf-1. The redox state of nitrosylated Cyt *c* released in apoptotic cells is not known,[6] but Cyt *c* may undergo conformational changes in both redox states. Conformational changes of Cyt *c* were evidenced through a different pathway involving the interaction with cardiolipin internally to mitochondria.[13,14,15] In apoptotic cells, a conformational change of Cyt *c* associated with mitochondria membrane was detected[16] whereas the binding of cardiolipin to Cyt *c* induces a strain leading to the cleavage of Fe−Met80 bond,[17] and furthermore, shifts the distribution of conformers population which is linked to its peroxydase activity.[14,18]

Nitric oxide is the sole gaseous ligand that readily binds to native Cyt *c*. A structural change in nitrosylated Cyt *c* is reminiscent of gas-sensors experiencing a conformational

change as a consequence of the cleavage of the stabilizing iron-methionine bond induced by NO binding.[19] In order to bind NO, the thermally driven cleavage of the iron-methionine bond must take place transiently in native Cyt *c*, an effect which was probed by absorption[20] and EPR measurements.[21] Thus, an equilibrium exists between the six-coordinated (6c-His-Met) and five-coordinated (5c-His) forms of the heme. Indeed, the breaking of Fe−Met bond is induced by a small pH increase with pK_a in the range 8.7 − 8.5 and with transition temperatures in the range 42 − 55 °C for ferric Cyt *c* from mammal species,[20] corresponding to low dissociation energy of 4.18 − 4.85 $kJ \cdot mole^{-1}$, which is slightly larger for the ferrous state of the heme (> 10 $kJ \cdot mole^{-1}$).[21] These properties rationalize the binding of NO to both redox states of Cyt *c*. We must also note that in controlled conditions (especially the pH), ferric Cyt *c* may catalyze the nitrite production from NO,[22] but the reverse reaction also takes place from the ferrous nitrosylated form.[23]

Conformational changes are associated with physiological properties of Cyt *c*, depend on redox state of the heme and were demonstrated for Cyt *c* interacting with anionic lipids, with membrane, and upon precisely localized chemical modifications.[24] Particularly, it experiences the so-called alkaline transition (pKa = 9.3), the heme remaining six-coordinate from His-Fe-Met to His-Fe-Lys.[1,24] Of particular importance, the binding of NO to horse Cyt *c* induces the decrease of the rate of electron transfer to thiols by factors of 10^2 to 10^4. due to both conformational reorganization and to change in electron pathway.[25]

Hence, besides its ubiquitous role in electron transfer, Cyt *c* can be considered as an endogenous heme-binding NO-receptor. In the "classical" NO-receptor soluble guanylate cyclase (sGC), the coordination state of the iron is crucial since the binding of NO triggers the enzymatic activity through the cleavage of the Fe-His bond. Contrary to five-coordinated sGC, the heme of Cyt *c* is six-coordinated in the resting state, with a proximal histidine (His18) and a distal methionine (Met80) being two axial internal ligands for the heme iron.[1] The latter is crucial to maintain Cyt *c* redox potential.[26] The reactivity of these enzymes depends upon the properties of the heme iron which are modulated by coordination with side-chains and by the surrounding protein architecture. NO binding to Cyt *c* has several consequences: firstly, it locks the distal heme pocket in a configuration imposed by the Fe−Met80 bond cleavage, precluding the Met80 rebinding; secondly, it inhibits the peroxydase activity.[27] Furthermore, structural differences exist between the ferric and ferrous states.[28]

Here we investigate the conformational changes and the coordination dynamics of the heme of mitochondrial horse heart Cyt *c* upon interaction with NO, both in its ferrous and

ferric states. First we compared the equilibrium nitrosylated structures by Raman spectroscopy, then we probed the heme dynamics and reactivity upon NO photo-detachment by time-resolved resonance Raman spectroscopy (TR^3) with subpicosecond resolution and by transient absorption spectroscopy in a time range from picosecond to second. The appearance of the photoinduced 5-coordinate species is followed by ultrafast NO geminate rebinding (ps), then by the rebinding of distal Met80 after the exit of remaining NO molecules from the heme pocket (μs) and then by NO bimolecular rebinding (ms to s). We found that the ferrous and ferric states of nitrosylated Cyt *c* have different dynamics and reactivity reflecting their structural differences within the heme and its environment. The heme structural distortions (first of all ruffling) appear as a major parameter controlling the properties of the nitrosylated Cyt *c*, in line with its role in the interaction with anionic lipids[27,14] and in apoptosis.[6]

Experimental procedures

Samples preparation

Mitochondrial Cyt *c* (horse heart) was purchased from Sigma-Aldrich. Its purity was verified by HPLC and it was used without further purification for transient absorption and non-resonance Raman measurements. For resonance Raman studies, Cyt *c* was further purified by gel filtration (isocratic elution with 100 mM TEA buffer, pH 7.4 on Sephadex G25 and Akta Purifier, GE-Healthcare). The fractions of the main eluted peak absorbing at 410 nm were concentrated by ultra-filtration (5 kDa cut-off membrane, Millipore).

For transient absorption studies, the solution of ferric Cyt *c* (100 μL, ~50 μM in 10 mM TEA buffer, pH 7.4) was put in a 1-mm optical path length quartz cell (Hellma) sealed with a rubber stopper and degassed by means of four successive cycles of vacuum and purging with pure argon. The ferrous heme was obtained by addition of 10 μL of degassed sodium ascorbate solution (2 mM final concentration). For preparing ferrous NO-liganded Cyt *c*, gas phase 100% NO (Air Liquide) was directly introduced into the spectroscopic cell (total pressure of 1.2 bar, yielding 2.4 mM of NO in the aqueous phase). For preparing both ferric NO-liganded Cyt *c*, gas phase 100% NO or 10% NO diluted in pure N_2 (Air Liquide) was used, yielding 2.4 mM and 0.24 mM of NO in the aqueous phase, respectively. Equilibrium spectra were recorded at each step for monitoring the evolution of heme iron coordination state via the Soret-band shift. The absorbance of the sample, measured with a UV-1700

Shimadzu spectrometer, was in the range 0.5–0.8 at the Soret maximum for 1-mm path length.

For steady-state Raman and TR^3 measurements, the solution of Cyt *c* was prepared with 350-500 μM concentration in TEA buffer (10 mM; pH 7.5). The concentration was verified by measuring the absorbance at 530 mM (ε = 12 000 $mole^{-1}\cdot L\cdot cm^{-1}$) in a 1-mm optical path length quartz cell (OD of ~0.35−0.5). The sample (1.2 mL) was placed in a large-volume cylindrical quartz cell (Hellma 540-135-QS) closed with a rubber stopper and degassed. Ferrous Cyt *c* was prepared by injecting the degassed sodium ascorbate (60 μL, 5 mM final concentration) directly into the cell. Nitrosylated complexes of both ferric and ferrous Cyt *c* were prepared by injection after vacuuming, of 100% NO (at 1.3 bar) into the cell through the stopper, yielding 2.4 mM NO in solution. For steady-state non-resonance Raman measurements, sample preparation procedure was the same, however the samples were placed in a standard rectangular 1-cm quartz cell with a magnetic stirrer for solution mixing. All experiments were performed at room temperature.

Steady-state resonance Raman spectra

Resonance Raman spectra with continuous wave excitation (CW-RR) were recorded using a He-Cd laser and the same Raman setup as for TR^3 studies[29] (see below). The excitation wavelength of 441.6 nm has been chosen specifically to closely match the probe beam wavelength (435 nm) in TR^3 experiments. During the measurements, samples were contained in a spinning cylindrical quartz cell whose rotation speed was adjusted to produce a thin sample layer at the inner wall[29] and to assure the absence of noticeable photoinduced changes in the spectra of nitrosylated complexes. Spectral resolution was estimated better than 5 cm^{-1}.

Steady-state non-resonance Raman spectra

CW Raman spectra in non-resonant conditions were measured using a specially constructed NIR-Raman spectrometer[30] with the 780-nm excitation provided by a cw Ti:Sapphire laser (Spectra Physics, model 3900S) pumped by an argon ion laser (Spectra Physics, model 2017) working in all-lines mode (pump power 4 W). Samples were contained in a spectrophotometric 1×1×4 cm^3 quartz cell with a small magnetic stirrer for fast solution mixing. Raman signal was collected in backscattering geometry with respect to the excitation beam using a 10× objective (Olympus MA10, NA 0.25) and directed through a spectrometer (Acton SpectraPro 2500i) into a liquid-nitrogen cooled back-illuminated NIR-sensitive CCD detector (Princeton Instruments SPEC-10 400BR/LN). Raman frequency calibration was

performed using toluene lines with an absolute accuracy of ±2 cm^{-1} and relative accuracy of ±1 cm^{-1}. Spectral resolution was 5 cm^{-1}.

Time-resolved resonance Raman spectra

Time-resolved sub-picosecond Raman apparatus has been described in detail elsewhere.[29] Briefly, it is based on a femtosecond Ti:Sapphire oscillator and a regenerative amplifier (output beam parameters are: wavelength 810 nm, pulse energy ~0.6 mJ, pulse duration 100 fs, repetition rate 1 kHz) and has 0.7-ps temporal resolution and 25-cm^{-1} spectral resolution. An optical parametric generator and two optical parametric amplifiers allowed to generate the photodissociating pump pulse (560-570 nm; 2 μJ; ~100 fs), whose delay was controlled by a translation stage, and the Raman probe pulse (435 nm; 25 nJ; 0.7 ps duration; 25 cm^{-1} spectral width). Both beams were collinearly overlapped by a dichroic mirror. Sample illumination and signal detection was performed in 90° geometry, with excitation coming from the bottom of the spinning cylindrical quartz cell. The detection was performed with a liquid-nitrogen cooled back-illuminated deep-depleted CCD (Princeton Instruments SPEC-10 100BR/LN) at the output of a 1-m focal length spectrometer (Jobin-Yvon HR1000). Raman frequency calibration was performed using Kr and Xe spectral lamps (Oriel) with an absolute accuracy of ±2 cm^{-1} and relative accuracy of ±1 cm^{-1}. Raman intensity normalization was made using the 980 cm^{-1} line of ammonium sulfate added as a reference to buffer solution.

The procedure for obtaining the pure photoproduct spectra from raw TR^3 data has already been described in detail elsewhere.[29] All Raman spectra presented in Fig 1-8 were corrected on slowly changing background due to Rayleigh scattering and residual fluorescence using a cubic spline interpolation in Igor Pro software.

Picosecond transient absorption

Ultrafast transient absorption (TA) measurements were performed with the pump-probe laser system previously described.[31] The photo-dissociation of NO was achieved by an excitation pulse centered at 564 nm, in the maximum of the $Q_{0\text{-}0}$-band absorption, with duration of ~40 fs and a repetition rate of 30 Hz. The broad-spectrum probe pulse was generated from a H_2O-cell continuum and was used to monitor the transient absorption changes within the Soret-band in the range 375–500 nm as a function of delay between pump and probe pulses. The optical path length of the cell was 1 mm. The sample was continuously moved perpendicularly to the laser beam and the temperature was 18 °C. Successive transient spectra as a function of time were recorded with a cooled CCD detector (EGG Princeton

Applied Research), forming a time-wavelength data matrix. Analysis of the data was performed by singular value decomposition (SVD)[31,32] of the time-wavelength matrix such that all transient spectral components were identified in the time window 0.5 ps–5 ns. Up to 40 scans were recorded and averaged with a dwell time of 1 s at each individual transient spectrum. The SVD kinetic components associated with SVD spectral components were fitted to the sum of a minimum number of exponential components. Alternatively, kinetics were also extracted at particular wavelengths from the raw data matrix.

Nanosecond to millisecond transient absorption

For this extended time-range we have used a home-built spectrophotometer comprising two lasers which were electronically synchronized and delayed.[33] The dissociating pulse of ~6 ns duration was provided by the second harmonic (532 nm) of a Continuum Nd:YAG laser. The probing pulses (6 ns FWHM) were provided by a tunable optical parametric oscillator (Panther, Continuum) pumped by the third harmonic of a Nd:YAG laser (Brilliant, Quantel) with a repetition rate of 10 Hz. The spectrometer was working in dual-channel mode, with both reference and probe channels equiped with optical fibers for light illumination/collection and diodes as detectors. The sample cell compartments and light collection design allowed recording signal variations $\Delta OD/OD$ as low as 10^{-5}. The kinetics of differential absorption changes were probed at particular wavelengths (absorption bands maxima and isosbestic points) by tuning the OPO. Up to twelve scans were averaged for each kinetics at a particular wavelength. Time delay after the dissociating pulse was changed linearly from 1 to 30 ns; it then was changed with a logarithmic progression from 30 ns to 1 s. The kinetics were globally fitted by using the same time constants for all probe wavelengths.

Results and discussion

Equilibrium structures

Resonance Raman spectra of equilibrium Cyt c species. The continuous wave resonance Raman (CW-RR) spectra of Cyt *c* in both ferrous and ferric redox states were measured with excitation at 441.6 nm and the native (His–Fe–Met) species were compared to their respective nitrosylated forms (His-Fe-NO) (Fig. 1 and 2). The assignment of Raman bands was made according to Hu *et al.*[34] and is given in Table 1. These spectra disclose numerous bands which are sensitive to the coordination, oxidation and spin states of the

heme[34] and some of them are also indicative of the heme non-planarity and structural distortions.[35]

The CW-RR spectrum of native ferrous Cyt *c* (Fig. 1a) agrees well with published spectra,[13,34,36] within the accuracy of absolute wavenumber calibration (±2 cm^{-1}), and we focus here on the changes induced by NO binding (Fig. 1b). First of all, for nitrosylated ferrous Cyt *c* we note the appearance of photoinduced spectral changes caused even by very weak CW excitation of a few hundred of microwatts at 442 nm. Therefore the extreme care has been taken in both using microwatt laser powers and subtracting the minor residual photoinduced contribution of His–Fe(II)–Met species from the overall experimental spectrum, in order to characterize the pure nitrosylated His–Fe(II)–NO species.

For both native and nitrosylated ferrous Cyt *c* the prominent ν(Fe–His) stretching band around 220 cm^{-1} is not visible, since this mode is not resonantly enhanced for 6-coordinate hemes with the Fe atom located in the heme plan.[37] The low intensity $\nu_{(Fe\text{-}S)}$ stretching mode has been detected at 351 cm^{-1} for the oxidized cytochrome P450[38] and at 347 cm^{-1} for chloroperoxidase.[39] For the native ferrous Cyt *c* (His–Fe(II)–Met) a sharp band centered at 345 cm^{-1} is present (Fig. 1a) while it transforms to a shoulder for the nitrosylated (His–Fe(II)–NO) species (Fig. 1b). Normally this band is attributed to the porphyrin ν_8 mode. Its disappearance or shifting upon NO binding may be partially related to the Fe–S bond disruption; this assignment must however be verified in future isotopic substitution experiment.

Next, the complex multiband contour within 350–430 cm^{-1} does not change much its shape upon Cyt *c* interaction with NO, within the accuracy of our measurements. The most prominent change in the low-frequency range however is a substantial intensity increase of out-of-plane (oop) symmetric pyrrole folding mode γ_{21} at ~567 cm^{-1} with respect to other adjacent modes and to this mode in the spectrum of native ferrous Cyt *c*. This band is known to be a ruffling distortion marker for *c*-type heme;[33] its intensity is related to the complex non-planar heme distortions, with ruffling deformation being the dominant one,[33,40] due to specific thioether linkages with Cys residues of the apoprotein structure. Hence, our Raman data indicate that sustantial heme ruffling is present in the native protein, being further enhanced in the nitrosylated ferrous Cyt *c*. Interestingly, the conformation of His–Fe(II)–Met80 species is partially determined by the distal link between Fe(II) and the protein via the methionine, so that the heme is expected to become less distorted upon the replacement of Met80 by NO, decoupling the heme from its distal constraint. However, this is not the case: our data reveal the increase of ruffling distortion upon nitrosylation of ferrous Cyt *c*.

Heme ruffling is a pyrrole-ring torsion with respect to the Fe-N_{pyr} bond axis. It changes the electron density in molecular orbitals and modulates the heme redox potential, as shown for Cyt *c*[35] and bacterial heme-sensors,[41] in line with a direct measurement of the change of redox potential of the heme upon NO binding.[25] In ferrous Cyt *c* the change of heme distortion after NO binding is correlated with the ease of Fe–Met80 bond breaking which is facilitated by simultaneous binding of NO and anionic lipids such as cardiolipin.[14,42]

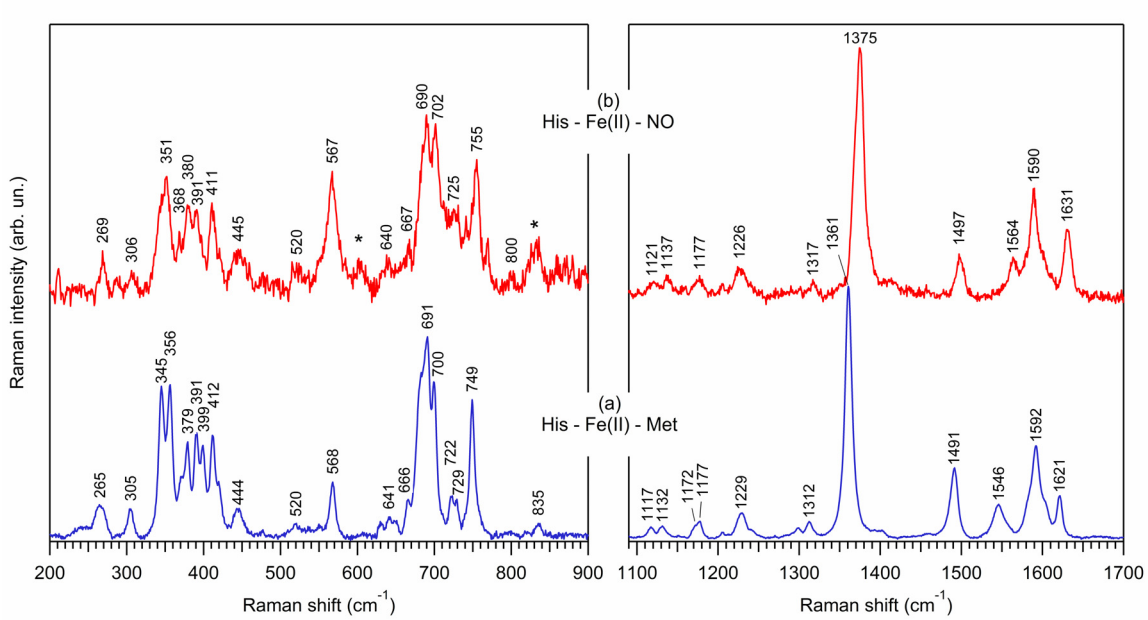


Fig. 1. CW-RR spectra of mitochondrial horse heart ferrous Cyt *c* (traces a) and its nitrosylated complex (traces b). Excitation wavelength 441.6 nm. Laser power was 2 mW for native Cyt *c* (accumulation time 5 min), and 50 – 400 μW for nitrosylated complex (accumulation time 20 min). Small photoinduced contribution of His–Fe(II)–Met species in the spectrum of His-Fe(II)-NO complex has been removed by weighted subtraction. Asterisks denote the residual ascorbate contribution. Assignments are given in Table 1.

In the high-frequency range (Fig. 1b), the prominent oxidation state and π-electron density marker band ν_4 experiences large frequency upshift from 1361 to 1375 cm^{-1} upon NO binding indicating rather large change in electronic distribution for a low-spin six-coordinate heme (His–Fe^{2+}–NO). The frequencies of other marker bands[43] ν_2, ν_3, ν_{11} and ν_{10} correspond well to a small core size and low-spin state of the 6c heme iron, whatever the nature of the distal ligand, Met80 or NO. We note, however, that the bands ν_3, ν_{11}, and ν_{10} experience variable upshifts upon Met80→NO exchange (1491→1497 cm^{-1}, 1546→1564 cm^{-1}, and 1621→1631 cm^{-1} respectively), while the band ν_2 experiences small downshift (1592→1590 cm^{-1}). A complicated interplay of electronic and structural perturbations of the ferrous heme upon NO binding could be a possible reason for such a contrasting behavior of high-frequency Raman markers.

Table 1. Assignment and band frequencies (cm^{-1}) in Raman spectra of ferrous and ferric Cyt *c* and their nitrosylated complexes recorded with excitation at 441.6 nm (data from Fig. 1, 2 and 5).

Mode assignment	Ferrous Cyt *c*	Ferrous Cyt *c* –NO	Ferric Cyt *c*	Ferric Cyt *c* –NO
γ_{24}	–	–	230	238
ν_9	265	269	268	268
ν_{51}	305	306	303	(vw)
ν_8	345	351 (merged)	347	343 - 349
ν_{50}	356		358	–
δ(C–C–C)	379	380	380	378
δ(C–C–S)	391-399	390	396	395
δ(C–C–C)	412	411	412	416
γ_{22}	444	445	444	444
ν_{33}	(vw)	(vw)	479	(vw)
γ_{12}	520	520	522	519
γ_{21}	568	567	566	553 + 567
ν_{48}	641	640	653	642
γ_{20}	666	667	(sh)	666
ν(C–S)	691	690	690	695 (merged)
ν_7	700	702	700	
γ_{11}	722	725 (bc)	711	(sh)
γ_5	729		729	(vw)
ν_{15}	749	755	744	751
ν_6	(vw)	800	798	800
γ_4	–	(*)	823	(vw)
γ_{10}	835	833	837	–
γ_{19}	–	–	855	–
ν_5	1117	1121	1124	1123
ν_{14}	1132	1137	1129	1136
ν_{30}	1172	1177 (merged)	1168	1171
–	1177		1178	1179
ν_{13}	1229	1226	1232	1229
δ(C–H)	1300 (vw)	-	1302	1303
$\nu_{21} + \delta$(C–H)	1312	1317	1316	1317
ν_4	1361	1375	1371	1376
ν_{29}	(sh)	(sh)	1410	(sh)
ν_{28}	(vw)	–	1466	(bc, vw)
ν_3	1491	1497	1501	1505
ν_{11}	1546	1564	1560	1566
ν_2	1592	1590	1583	1587
ν_{10}	1621	1631	1635	1638

vw: very weak band; sh: shoulder; bc: broad contour; (*): overlapped with ascorbate band.

In the CW-RR spectrum of native ferric Cyt *c* (Fig. 2a), the intense and sharp band located at 347 cm^{-1}, assigned to ν_8, is also present but weakened after NO binding (Fig. 2b), again suggesting a possible contribution of the $\nu_{(Fe\text{-}S)}$ stretching mode.[38,39] The triplet pattern at 380 – 412 cm^{-1}, assigned to $\delta_{(C\text{-}C\text{-}C)}$ and $\delta_{(C\text{-}C\text{-}S)}$ deformations is not influenced by NO binding. Remarkably, the oop rufling marker mode γ_{21} at 566 cm^{-1} appears sharp and intense for native ferric Cyt *c* but becomes very weak upon binding of NO, in stark contrast to the case of ferrous heme. The behavior of γ_{21} implies very strong non-planar heme distortion in native ferric Cyt *c*, larger than in the native ferrous state, in agreement with the heme ruffling deduced from low vibrational modes (40 – 300 cm^{-1}).[35,44] Such a stronger heme distortion in the native ferric form with respect to the ferrous one was also revealed in the iso-1-Cyt *c* by their compared X-ray structures.[45]

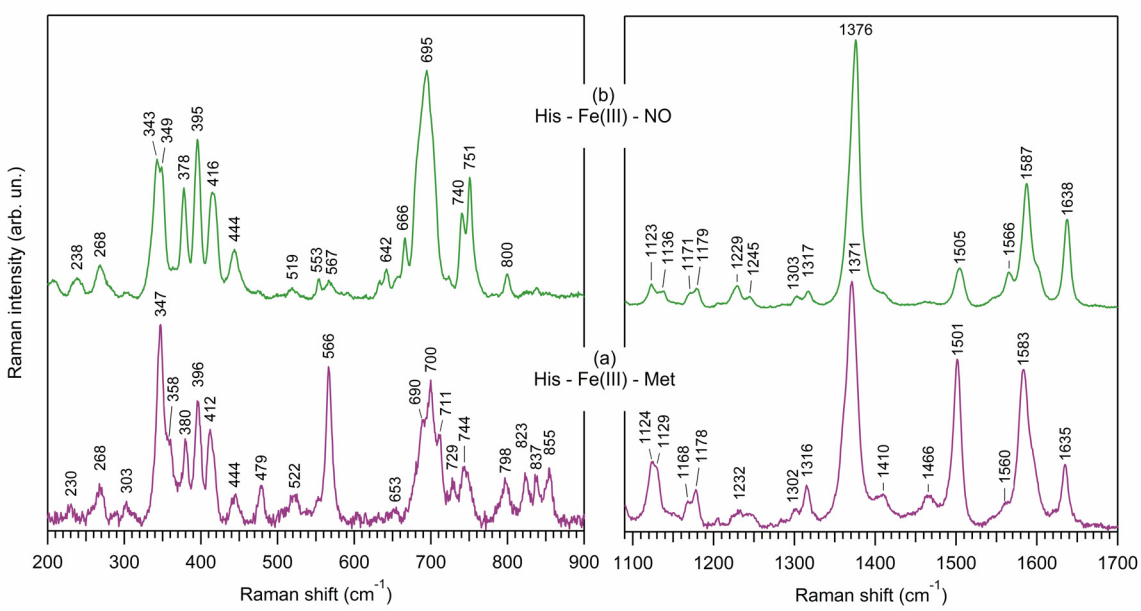


Fig. 2. The same as in Fig. 1, but for ferric Cyt *c*. Laser power was 2 mW for all spectra, photoinduced changes have not been observed. Accumulation time was 5 min in the high-frequency range and 10 min in the low-frequency range. Assignments are given in Table 1.

Concerning the nitrosylated ferric Cyt c, the mode ν_{33} at 479 cm^{-1}, which corresponds to in-plane pyrrole rotations, vanishes in the presence of NO, while many weak non-planar low-frequency Raman modes (γ_{22}, γ_{12}, γ_{21}, γ_{20}) are still discernible in Fig. 2b. These findings suggest that the heme macrocycle in His–Fe(III)–NO configuration is much less distorted although still not planar as compared to the very distorted native His–Fe(III)–Met80 structure. The conclusion is further supported by Raman bands transformation in 650 – 900 cm^{-1} region (Fig. 2). Indeed, we observe a down-shift of the band ν_7 from 700 to 695 cm^{-1} after NO

binding (becoming merged with the $\nu_{(C\text{-}S)}$ mode from the thioether heme-protein bond at 690 cm^{-1}), which is also sensitive to heme distortion.[46] Furthermore, the binding of NO induces an intensity increase of the band ν_{15} (751 cm^{-1}) together with its upshift and the remarkable disappearance of the triplet at 823 – 855 cm^{-1}, assigned to the C_m–H out-of-plane modes γ_4, γ_{10} and γ_{19} in the spectrum of native ferric Cyt *c*.

In the high-frequency range, the marker band ν_4 experiences a small upshift from 1371 to 1376 cm^{-1} upon NO binding (Fig. 2) again indicative of a low-spin 6c-NO nature of the ferric heme. This conclusion is further supported by the behavior of other marker bands, ν_2, ν_3, ν_{11} and ν_{10}, all experiencing rather small frequency upshifts upon NO replacing Met80.

Non-resonance Raman spectra of equilibrium Cyt c species. In an attempt to probe the effects of NO binding on the overall protein structure, we have also recorded the non-resonant Raman spectra of native and nitrosylated Cyt *c* with near-infrared excitation at 780 nm (Fig. 3 and 4; Table 2).

We first note that many heme modes dominate the spectra despite the non-resonant excitation conditions, which therefore can be better characterized as "pre-resonant". Non-totally symmetric B_{1g} modes (ν_{10} – ν_{15}) are predominantly enhanced, while totally symmetric A_{1g} modes are generally absent, with the exception of the mode ν_2 which is however rather weak. The positions and shifts of the porphyrin Raman bands observed with resonance excitation (Fig. 1 and 2) are well reproduced in non-resonant conditions, for both Cyt *c* redox states. Most conspicuously, the modes ν_{10} (1621 – 1638 cm^{-1}), ν_{11} (1546 – 1566 cm^{-1}), and ν_{15} (744 – 756 cm^{-1}) behave exactly as in resonant conditions. Concerning the heme ruffling distortion, the intensity changes of the oop marker γ_{21} in 565 – 568 cm^{-1} range, occurring in opposite directions for ferrous and ferric heme species (Fig. 1 and 2), are also detected with a 780-nm excitation (Fig. 3 and 4), confirming the difference in structural impact of NO binding to the heme iron.

Several characteristic Raman bands of the protein structure are observed. The doublet 822/828–851 cm^{-1} (Fig 3 and 4) is assigned to the four Tyr side-chains[47,48] being hidden in resonance conditions. Indeed, in the RR spectrum of ferric Cyt *c*, the triplet at 823–837–855 cm^{-1} due to γ_4, γ_{10} and γ_{19}, close to the Tyr bands, vanishes after NO binding and is absent in the resonant spectra of its ferrous form independently of NO (Fig 1 and 2). Contrastingly, the 823–850 cm^{-1} doublet from Tyr is present in non-resonance Raman spectra of both native and nitrosylated Cyt *c*, in both redox states without any change, indicating that nitrosylation does not perturb neither the environment of the Tyr phenol, nor the hydrophilic/hydrophobic character of interactions in which Tyr are involved.[48,49] In both oxidation states there is no

change for the Phe (1003 cm^{-1}), the protein bending $\delta_{(C\text{-}H2)}$ (1447 cm^{-1}) and the Amide I (1656 cm^{-1}) bands assigned to helical structure without β-sheet. In the ferric state, the intensity of the band at 1284 cm^{-1} due to mode $\delta(C_aH)_{2,4}$ increases after NO binding, showing some localized conformational changes of the side-chains. The frequency of Amide I in our steady-state Raman data very well matches that measured by transient IR spectroscopy which revealed a slight increase of its intensity upon NO dissociation but no shift.[50]

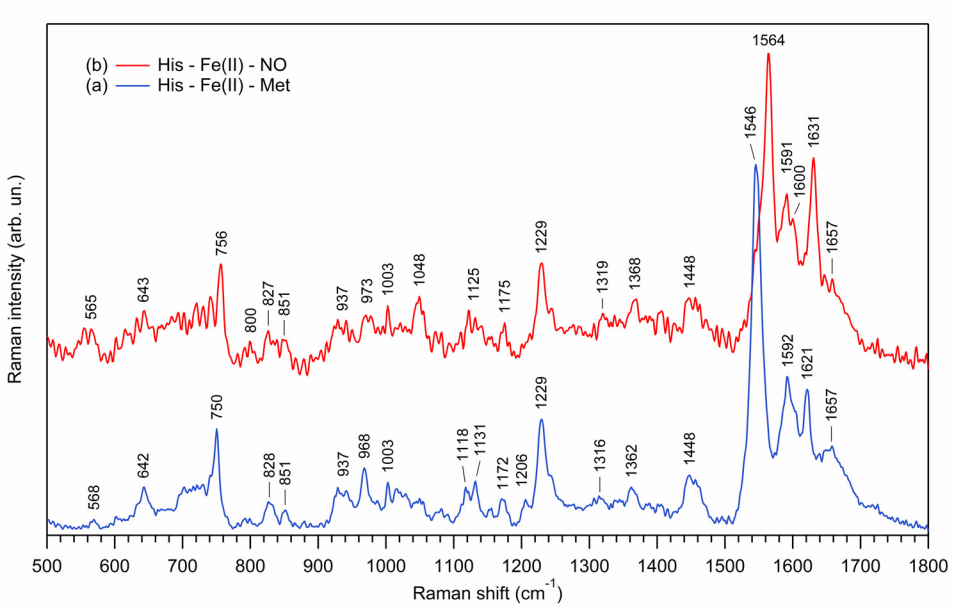


Fig. 3. CW non-resonance Raman spectra with excitation at 780 nm of mitochondrial horse heart ferrous Cyt *c* (trace a) and its nitrosylated complex (trace b). Laser power 100 mW, total accumulation time 20 min for native Cyt *c* and 50 min for its nitrosylated complex. Photoinduced changes were not observed. Water buffer contribution is subtracted. Assignments are given in Table 2.

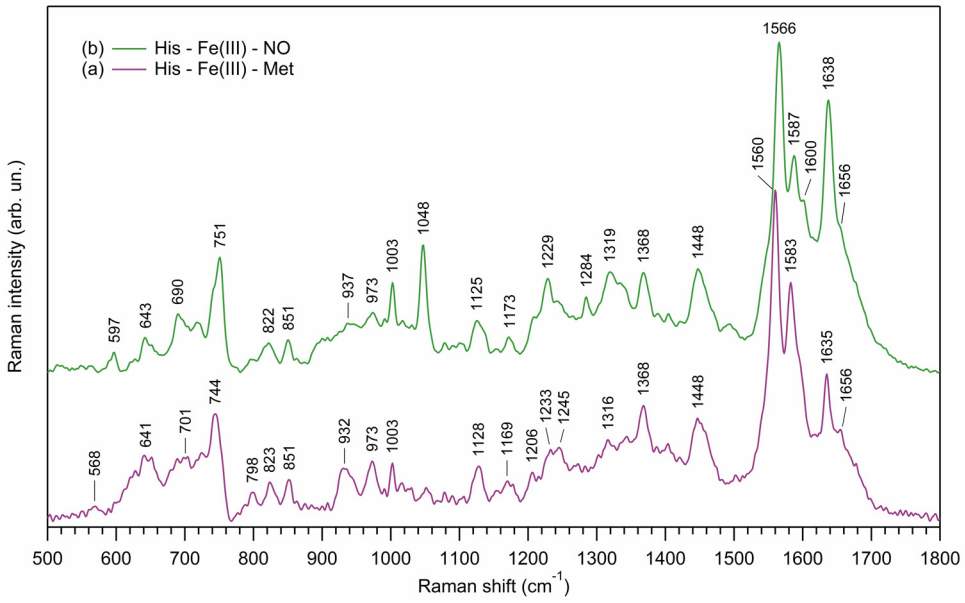


Fig. 4. The same as in Fig. 3, but for ferric Cyt *c*. Laser power 100 mW, total accumulation time 15 min for both spectra. Water buffer contribution is subtracted. Assignments are given in Table 2.

Overall, the non-resonance Raman spectra do not provide evidence of substantial changes of the secondary or tertiary apoprotein structure induced by heme nitrosylation in both oxidation states, while some rather weak changes localized to the heme and heme pocket have been observed. In the absence of NO, the native ferric and ferrous forms also differ only by the changes localized in the heme and its pocket, in agreement with the compared structures in both redox states of horse,[28] tuna,[51] and yeast[45] Cyt *c*.

Table 2. Assignment and band frequencies (cm^{-1}) in Raman spectra of ferrous and ferric Cyt *c* and their nitrosylated complexes recorded with excitation at 780 nm (data from Fig 3, 4 and 6).

Mode assignment	Ferrous Cyt *c*	Ferrous Cyt *c* –NO	Ferric Cyt *c*	Ferric Cyt *c* –NO
γ_{21}	568	565 (bc)	568	–
Tyr + ν_{48}	642	643	641	643
Thioether ν(Ca-S) + ν_7	(bc)	(bc)	701 (bc)	690 (bc)
ν_{15}	750	756	744	751
ν_6	(vw)	800	798	(sh)
Tyr	828	827	823	822
Tyr	851	851	851	851
ν_{46}	937 (bc)	928 (bc)	932 (bc)	937 (bc)
Backbone ν(Cα–C)	968	973 (bc)	973	973
Phe	1003	1003	1003	1003
$\nu_{sym}(NO_3^-)$	–	1048	–	1048
ν_5	1118	–	–	–
ν_{14}	1131	1125 (bc)	1128	1125 (bc)
Tyr + ν_{30}	1172	1175	1169	1173
Phe + Tyr	1206	(vw, sh)	1206	1208
ν_{13}	1229	1229	1233	1229
$\delta(CaH)_{2,4}$	–	(vw, bc)	–	1284
$\delta(CaH)_{2,4}$	1316	1319	1316	1319 (bc)
ν_{12}	1362	1368	1368	1368
Protein $\delta(CH_2, CH_3)$	1448	1448	1448	1448
ν_{11}	1546	1564	1560	1566
ν_2	1592	1591	1583	1587
ν_{37}	(sh)	1600	(sh)	1600
ν_{10}	1621	1631	1635	1638
Amide I	1657	1657	1656	1656

vw: very weak band; sh: shoulder; bc: broad contour.

Electronic and structural similarities and differences between redox states of nitrosylated Cyt c. Comparison of the porphyrin marker bands in the high frequency range for nitrosylated Cyt *c* (Fig. 5 right panel and Fig. 6) illustrates the consequences of NO binding as a function of the redox state. Several factors influence the intensities and the frequency positions of these markers: porphyrin core size, Fe spin state, Fe coordination state, heme structure distortions, and π-electron density distribution. Remarkably, the frequencies of the modes ν_4 and ν_{11} are very close for both redox states of nitrosylated Cyt *c*, while the mode ν_2 and especially the modes ν_3 and ν_{10} exhibit frequency differences beyond the accuracy of measurements ($3 \leq \Delta\nu \leq 8$ cm^{-1}). These frequency differences are however much less pronounced than in the case of the two redox states of native Cyt *c* ($\Delta\nu \leq 14$ cm^{-1}) (Table 1, columns 2 and 4). Such a behavior, especially of the electron density marker mode ν_4, indicates similar π-electron configurations of the porphyrin macrocycle for the heme–NO complex in both redox states.

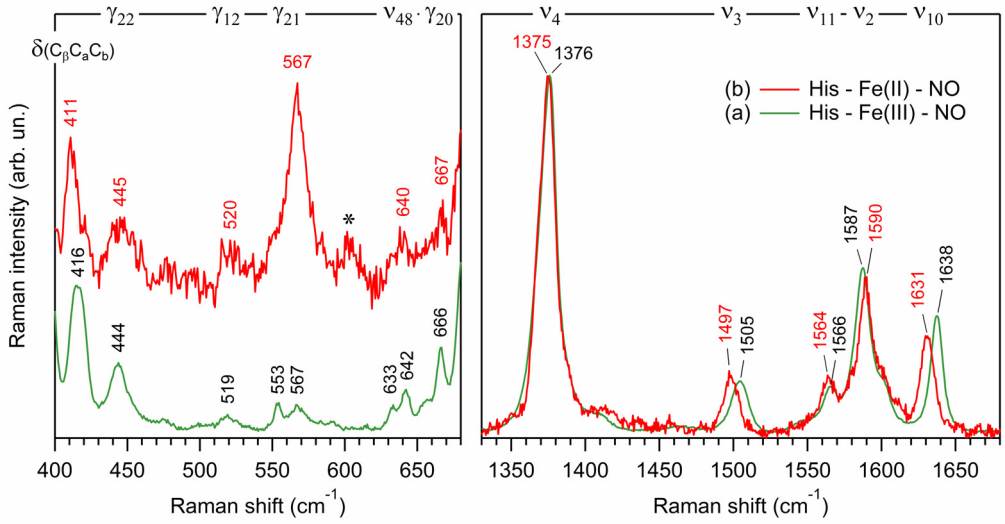


Fig. 5. Comparison of CW-RR spectra in characteristic frequency ranges of ferrous (b, red curves) versus ferric (a, green curves) forms of nitrosylated Cyt *c*, with excitation at 442 nm. The spectra were normalized and arbitrary shifted along the Raman intensity axis for visual convenience of bands comparison. Bands assignment is shown on top of both panels.

The frequency of the mode ν_4 is also the same for Fe(III)–NO and Fe(II)–NO in myoglobin[52,53] (Mb) and horse radish peroxydase[51] (HRP) and close to that of native proteins with ferric heme. We may conclude that the π-electron density of the porphyrin core is generally similar for ferric and ferrous nitrosylated hemes, both *b*- and *c*-types. However for Cyt *c* the pattern of modes ν_3 – ν_{10} retains its relative intensity ratios, contrary to Mb and HRP,[52] pointing out a much closer electronic configuration for the two redox states of Cyt *c*.

The shift of ν_4 frequency of the Fe(II)–NO Cyt *c* species (1375 cm^{-1}) toward the value characteristic for Fe(III) is explained by the iron d_π electron withdrawal from the porphyrin π^* orbitals,[54] mimicking the Fe(III) d-electron configuration, in the process of competitive bonding with NO π^* orbitals (so-called π-backbonding).[54,55] At the same time, the σ-bonding between π^* orbital of NO and d_{z2} orbital of low-spin Fe(II) which is orthogonal to the macrocycle plane, does not perturb the porphyrin π-electronic system and consequently does not change the ν_4 frequency. The exact electronic charge distribution for Fe(II)–NO *versus* Fe(III)–NO bonds in Cyt *c* cannot be infered from our data. However, the direct measurement of the ν(NO) stretching frequency (1922 cm^{-1}) for nitrosylated ferric Mb[56] revealed slightly electron deficient NO ligand resulting in a resonant species $Fe–N{\equiv}O^+$ and not the NO^- anion.[57] The true electronic configuration has consequences on NO dissociation: as noted by Hunt and Lehnert,[55] there could be an apparent contradiction between the very high dissociation energy barrier (~30 kcal·mol^{-1})[58] and the fast rate of NO dissociation (k_{off}) which is larger than that for the ferrous species. However, in ferric heme model the resonant species $Fe(II)–NO^+$ was shown to cross (within ~0.2 Å of the Fe–NO elongation) the two potential energy surfaces of the LS and HS Fe(III)–NO states, the latter one being dissociative.[58]

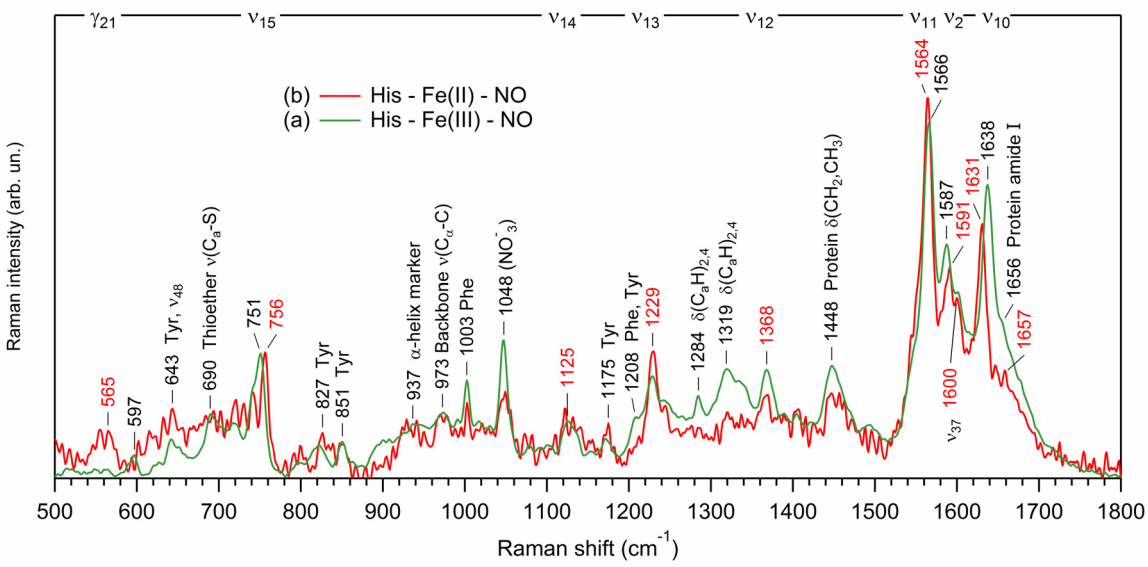


Fig. 6. Comparison of CW Raman spectra of ferrous (red curve) versus ferric (green curve) of nitrosylated Cyt *c*, with non-resonance excitation at 780 nm. The spectra were normalized for the convenience of bands comparison.

Another remarkable feature is the prominent change in the heme structure induced by NO binding, namely the drastic intensity decrease of the ruffling marker band[33] γ_{21} (symmetric pyrroles folding, 565-567 cm^{-1})[34] which almost vanishes for ferric Cyt *c* while

being strongly enhanced for the ferrous form (Fig. 5, left panel, and Fig. 6). The intensity of this band is directly proportional to the degree of ruffling distortion of the heme.[33] Noticeably, this band disappears for the membrane-bound Cyt *c*, having more planar heme structure,[35] suggesting a role in electron transfer for this conformational feature. This is exemplified by the peroxydase activity of Cyt *c* in the presence of anionic lipids correlated with the breaking of the Fe(II)–Met80 bond, in the absence or presence of NO.[14] The conclusion that the nitrosylated ferrous Cyt *c* possesses much more ruffled structure than its ferric analogue is corroborated by the frequency downshifts of the marker bands ν_3 and ν_{10} which are also sensitive to ruffling distortion.[42]

Importantly, several other oop Raman bands, namely γ_{20} (anti-symmetric pyrroles folding, 666 – 667 cm^{-1})[34] and γ_{22} (pyrroles swivel, 444 – 445 cm^{-1})[34] remain the same for both redox states (Fig. 5, left panel) suggesting that the heme macrocycle distortions other than ruffling are still present for the nitrosylated ferric Cyt *c*. On the other hand, the relaxation of heme distortion induced by NO binding to the ferric Cyt *c* is sustained by the disappearance of the oop γ_4, γ_{10}, γ_{19} (823 – 855 cm^{-1}) modes, a behavior not observed for nitrosylated ferrous Cyt *c*. We thus infer a decrease of the heme ruffling distortion[59] and a more relaxed heme conformation upon NO binding to ferric Cyt *c*, in contrast with ferrous Cyt *c*, which exhibits very strong non-planar ruffled heme distortion, in spite of similar π-electron density distribution for both redox states. We conclude that the heme macrocycle ruffling distortion evolves in opposite ways in ferric and ferrous Cyt *c* upon binding of NO to the heme iron at the distal location, replacing Met80, but these conformational changes are not driven by the Met80 detachment.

Ultrafast structural changes

TR^3 spectra of nitrosylated ferrous Cyt c. The TR^3 study of vibrational relaxation of native horse heart Cyt *c* in both oxidations states have already reported.[31] Structural dynamics of nitrosylated ferrous Cyt *c* has also been reported with the emphasis on retardation of the iron motion following NO geminate rebinding, via the picosecond intensity evolution of Fe-His Raman stretching band.[60] Here we report an extended TR^3 data set for nitrosylated Cyt *c* with the main focus on ultrafast heme structural changes after the event of NO dissociation.

TR^3 spectra of nitrosylated ferrous Cyt *c* in the first 25 ps after NO photo-detachment are presented in Fig. 7 and the corresponding bands assignment is given in Table 3. We emphasize that the transient difference Raman spectra at positive time delays represent the pure photo-product species since the contribution of the non-excited molecules was

subtracted, as already described.[29] These spectra disclose broader bands compared to CW-RR spectra due to the lower spectral resolution (25 cm^{-1}) of the 0.7-ps probing pulse.

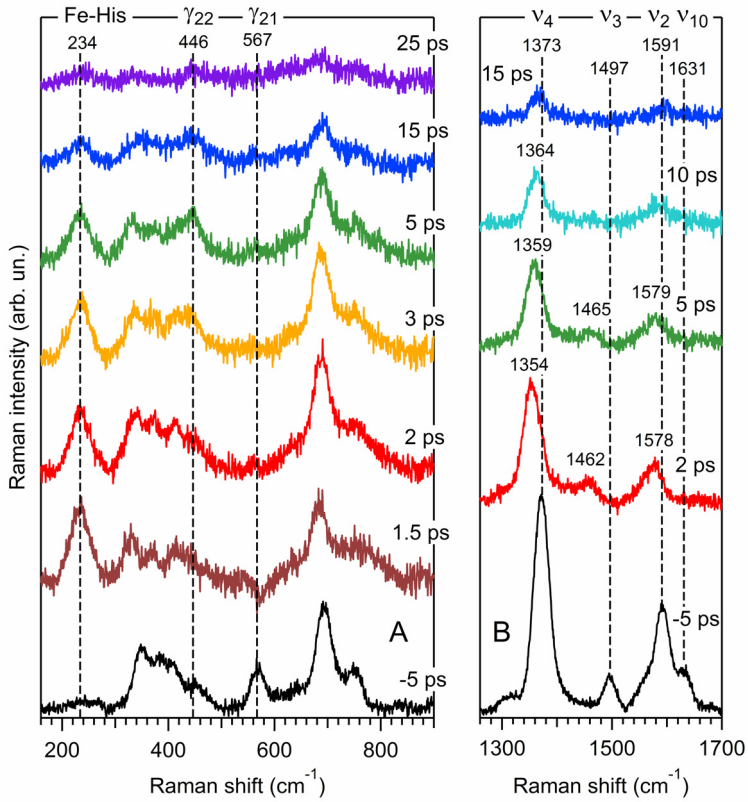


Fig. 7. TR^3 Raman spectra of nitrosylated ferrous Cyt *c*, at different time delays between pump and probe pulses. Traces at $\Delta t = -5$ ps correspond to measured spectra; traces at positive time delays are difference spectra representing the photoinduced transient species. The position of several characteristic Raman bands is outlined by vertical dashed lines. The assignments are given in Table 3.

In the high frequency range the ν_4 band appears shifted at time delay $\Delta t = +2$ ps, from 1373 to 1354 cm^{-1}, which is not its position for the native His–Fe(II)–Met 6-coordinate species (1361 cm^{-1}; Fig. 1a) but corresponds to that of a 5c-HS transient species after NO dissociation. The subsequent upshift of the mode ν_4 to 1364 cm^{-1} at +10 ps is due to heme vibrational and structural relaxations.[31] The mode ν_3, very sensitive to the heme out-of-plane distortions, is located at 1497 cm^{-1} in the ground state His–Fe(II)–NO (–5 ps) and experiences an immediate downshift to 1462 cm^{-1}, a value corresponding to a 5c-HS ferrous heme, as observed after the dissociation of NO from myoglobin[60] and hemoglobin[61] whereas it appears at 1491 cm^{-1} for the native 6c-LS His–Fe(II)–Met80 (Fig. 1a). Similar frequency downshifts of the mode ν_3 were also observed for other 5c-HS species like microperoxidase[36] or a fragment of ferrous Cyt *c*.[62] Similarly, the mode ν_2 at 1590 cm^{-1} shifts to 1578 cm^{-1} and simultaneously decreases in intensity as observed for myoglobin.[60] Lastly, the band ν_{10} at 1631 cm^{-1} disappears, in agreement with the high spin nature of the heme after NO

dissociation. Thus, the photoproduct spectra in Fig. 7 correspond to the transient 5c-HS His–Fe(II) Cyt *c* and their overall decrease in intensity with time is due to the reformation of the ground-state 6c-LS species His–Fe(II)–NO in picoseconds, through NO geminate rebinding, and not Met80 rebinding, for the major part (~98%, see below) of the photo-dissociated molecules.

In the low frequency range, the spectral evolution of the ferrous Cyt *c* shows remarkable features (Fig. 7A). The appearance of the ν(Fe–His) stretching mode at 234 cm^{-1}, which is resonantly enhanced only for a non-planar ferrous heme[37,63] and appears transiently in Cyt *c*, reveals the heme doming induced by NO dissociation.[60] The ruffling marker γ_{21} at 567 cm^{-1} vanishes immediately after NO dissociation, indicating a relaxation of ruffling distortion in the transient His-Fe(II). The in-plane mode ν_8 downshifts from 345 to 335 cm^{-1}, which is not its frequency neither for His–Fe(II)–Met (Fig. 1a) nor for His–Fe(II)–NO (Fig. 1b) species. The modes $\delta_{(C\text{-}C\text{-}C)}$ and $\delta_{(C\text{-}C\text{-}S)}$ within the pattern at 360–420 cm^{-1} and more notably the out-of-plane pyrroles swivel mode γ_{22} at 446 cm^{-1} change their relative intensities with the laps of time from 1.5 to 25 ps. All together, these spectral changes reflect complicated heme macrocycle structural rearrangement after NO dissociation.

Table 3. Assignment and bands frequencies (cm^{-1}) in TR^3 spectra of nitrosylated ferrous Cyt *c*, presented in Fig 7 and 8.

Mode assignment	Ferrous Cyt *c* –NO		Ferrous Cyt *c* (b)
	Ground state	Photoproduct at 2 ps	Photoproduct at 2 ps
ν(Fe–His)	–	234	216
ν_8	345 (merged)	335 (merged)	333 (merged)
ν_{50}			
δ(C–C–C)	370	374	372
δ(C–C–S)	400	–	
δ(C–C–C)	412	414	411
γ_{22}	450	446 (bc)	–
γ_{21}	567	(vw)	–
$\nu(C_a\text{–}S) + \nu_7$	694	688	685
ν_{15}	750	751 (bc)	764 (bc)
ν_4	1373	1354	1345
ν_3	1497	1462	1454
ν_2	1591	1578	1571
ν_{10}	1631	–	–

(a) vw: very weak band; sh: shoulder; bc: broad contour.
(b) from Ref. 31 and 64.

In the case of ferric nitrosylated Cyt *c*, the 5-coordinate species produced after NO photodissociation exhibits a Soret transient absorption maximum around 390 – 400 nm (see TA data below) and cannot be efficiently probed by TR^3 with excitation at 435 nm. Indeed, the resulting transient Raman spectrum (data not shown) is dominated by vibrationally excited 6-coordinated nitrosylated ferric Cyt *c*, while the contribution from the five-coordinate species is impossible to separate due to lack of resonance enhancement. The photodissociation of NO from the ferric heme was nevertheless confirmed and probed by TA (see below).

Ultrafast dynamics of 5-coordinate heme structure after NO dissociation. The transient 5c-HS species can be produced by photodissociation of either NO or Met80.[31,64] First we note one important similarity between their respective transient spectra (Fig. 8): the disappearance of the ruffling marker band γ_{21} at 567 cm^{-1}. This is an evidence of the immediate structural rearrangement of the 5C-HS species following the detachment of the sixth distal ligand, which is dominated by the heme doming and results in suppression of ruffling distortion for both NO and Met80, the heme being decoupled from distal constraints, but not from cysteine links with apoprotein structure.

We discuss now the following interesting and unexpected finding concerning transient 5c ferrous Cyt *c* species. Despite the general similarity of TR^3 spectra at Δt = +2 ps, several porphyrin marker band frequencies, together with the ν(Fe–His) band position and intensity of the 5c-HS His-Fe(II) species after NO photodissociation differ substantially from those of the same 5c-HS species but produced after Met80 photodissociation[31] (Fig. 8, Table 3).

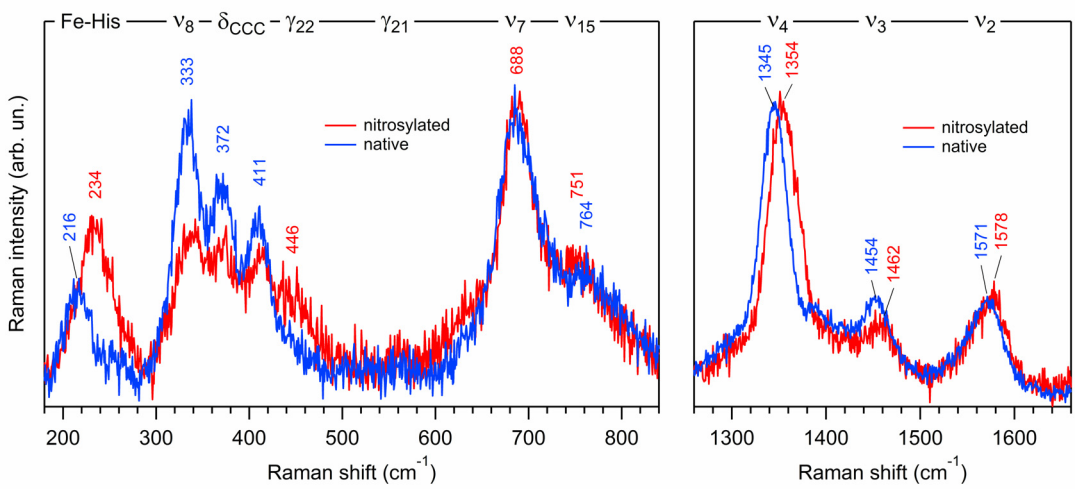


Fig. 8. Comparison of TR^3 difference spectra at time delay Δt = 2 ps between pump and probe pulses, for transient five-coordinate species obtained after NO photo-detachment from nitrosylated ferrous Cyt *c* (red curves), and Met80 photo-detachment from native ferrous Cyt *c* (blue curves, from Ref. 31).

Since at a few picosecond time delay the heme structure is not fully relaxed yet, we infer the following origins of the observed phenomenon. The initial equilibrium heme structures, nitrosylated His–Fe(II)–NO *versus* native His–Fe(II)–Met80, are subject to different non-planar distortions, the nitrosylated heme being more ruffled one (Fig. 1). Consequently, the non-equilibrium transient species produced immediately after the distal ligand detachment must also start from and evolve into different conformations. Moreover, the nearest environment in the heme pocket is also different for these two distal ligands. Thus, spectral differences are expected for Raman bands sensitive to oop heme macrocycle distortions in the range 300 – 650 cm^{-1}. Time evolution (Fig. 7A) of the mode γ_{22} at ~446 cm^{-1}, present only for the nitrosylated Cyt *c*, is especially revealing, as it directly demonstrates the macrocycle structural rearrangement with time for 5C-HS heme. Supporting the equilibrium data, these transient spectra prove that the 6-coordinate species His–Fe(II)–NO and His–Fe(II)–Met80 do not possess similar heme conformation.

It is known that the frequency of iron-histidine stretch ν(Fe–His) decreases upon increase of the iron oop displacement.[37] Hence, a large difference in ν(Fe–His), which is 234 cm^{-1} after NO dissociation and 216 cm^{-1} after Met80 dissociation (Fig. 8), reveals that the central iron is displaced much further away from the heme plane towards proximal histidine in the case of methionine detachment. Since the total excitation energy is provided by the same photodissociative ~100-fs pulse at 565 nm in both cases, the effect may originate from the difference in energy required to break the distal Fe–Met80 bond as compared to Fe–NO bond. From the proximal side, the ν(Fe–His) position may also be influenced by the initial Fe-His bond strength of the equilibrium 6C-LS heme. Large ν(Fe–His) upshift of 18 cm^{-1} is indicative of a weaker Fe-His bond for nitrosylated ferrous Cyt *c* as compared to the native protein.

An analogous effect was reported for soluble guanylate cyclase and its isolated β_1 heme domain, which exhibit ν(Fe–His) at 204 and 213 cm^{-1} respectively, immediately after CO photodissociation,[65] the latter structure of β_1 heme domain being less constrainted.[66]

In the high-frequency range (Fig. 8, right panel), all Raman markers for the 5C-HS species of native protein at Δt = 2 ps are systematically downshifted with respect to the nitrosylated complex, a behavior due to structural differences in the initial equilibrium 6C structures (Fig. 1).

Heme coordination dynamics after NO dissociation.

We studied the complete picture of heme coordination dynamics after the triggering event of NO photodissociation, from picosecond to second by time-resolved absorption. The structural events which occur in the picosecond to nanosecond time range differ from those occurring in the microsecond to second time range, we will describe successively the heme dynamics in these two time ranges, as they were recorded with two different TA techniques, for both redox states of nitrosylated Cyt *c*.

Ultrafast heme coordination dynamics in the picosecond time range. *Ferrous Cyt c–NO*. The binding of NO to ferrous Cyt *c* induces only a small shift (–3.5 nm) of the Soret maximum (Fig. 9A). The event of NO photodissociation is identified by the intense Soret-band bleaching which appears immediately at 412 nm accompanied by two induced absorption bands on each side (Fig. 9B). These spectral features decrease rapidly within the 500-ps time range. The *time* × *wavelength* matrix of induced absorptions (containing all transient spectra) was analyzed by singular value decomposition (SVD) yielding a main spectral transient component which is conspicuously different from the equilibrium difference between the spectra of native and nitrosylated Cyt *c* (Fig. 9C). The induced absorption band centered at 432 nm is characteristic of a ferrous five-coordinate heme and the induced band at 375 nm corresponds to the change of the δ band. Consequently, the decrease of this transient spectrum with time is due to geminate rebinding of photodissociated NO, with the kinetics being fitted by a multiexponential function (Fig. 9D). The fast initial phase (τ_{ex} = 2.5 ps) corresponds to the relaxation of vibrational excited states of the heme[31] and will not be further discussed. The geminate rebinding of NO to the 5c-His heme occurs in two phases having well separated time constants (τ_{G1} = 9.2 ps and τ_{G2} = 55 ps) and contrasted relative amplitudes (A_1 = 92.7% and A_2 = 5.7%). The time constant of NO geminate rebinding measured by IR transient spectroscopy[50] (7 ps) appears slightly faster than our value τ_{G1}, similarly to what is observed in the case of myoglobin.[67,60] The difference between the time constants from IR and TA experiments is explained by a delay between the Fe–NO interaction (probed by the NO stretch) and the subsequent stabilization of the electronic orbitals of the heme following NO binding (probed by transient absorption).[60]

Importantly, fitting over the entire 0.5-ns time range yielded a constant component (A_C = 1.5%) which reveals the proportion of NO exiting from the heme pocket and the protein core. After 0.5 ns the induced absorption spectrum keeps the same shape and no other process is detected up to 5 ns. (previously,[60] a shorter recorded time range did not allow to observe the 55-ps component with small amplitude).

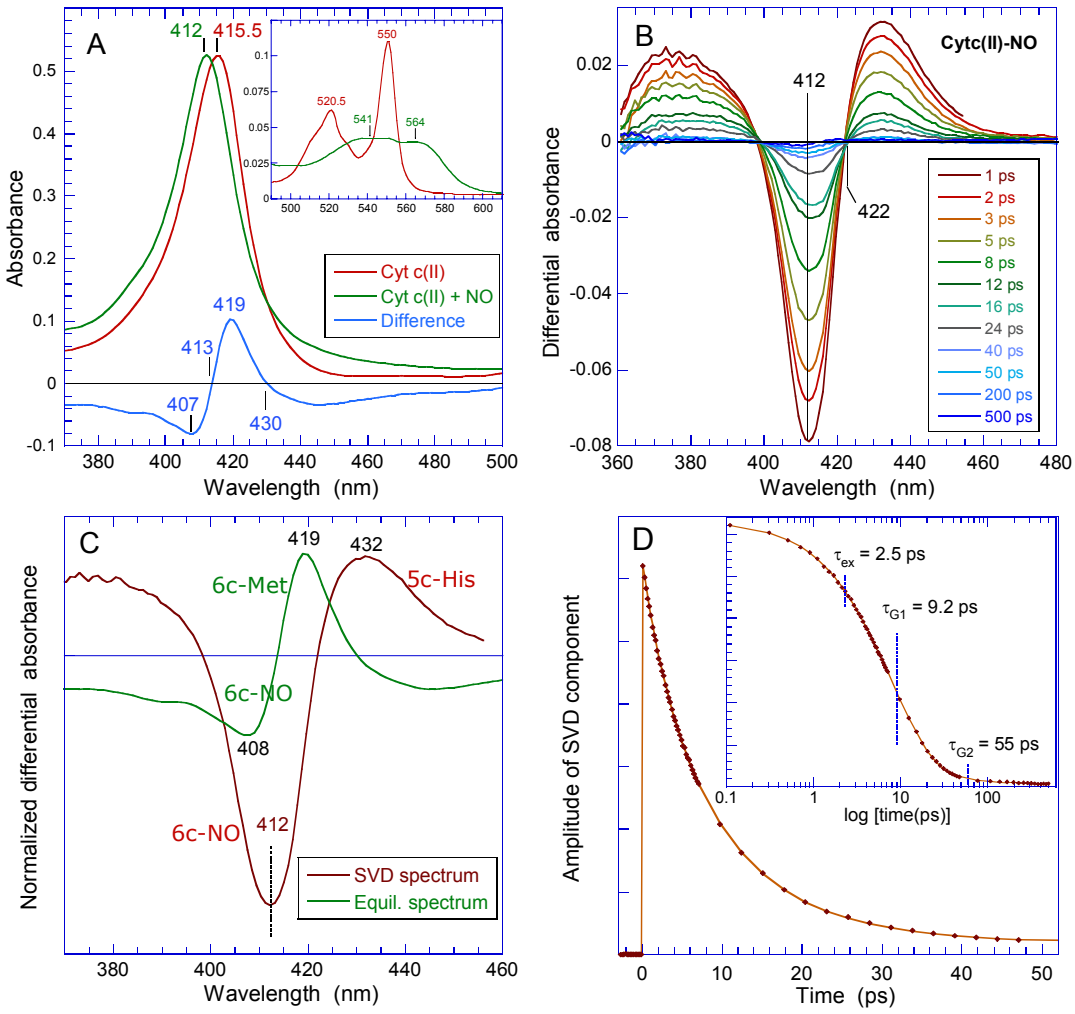


Fig. 9. (A) Equilibrium spectra of ferrous Cyt *c* with and without NO. (B) Differential transient spectra of ferrous Cyt *c* at various time delays after photodissociation of NO. (C) The main SVD spectral component globally extracted from all transient spectra is compared with the steady-state difference. The coordination states of the heme are indicated. (D) Fitted kinetics of the SVD spectral component with the position of time-constants displayed on a log scale.

Ferric Cyt c–NO. The Soret-band maximum of native ferric Cyt *c* (408.5 nm) is characteristic of 6-coordinate ferric hemes and shifts to 416.5 nm upon the binding of NO (Fig. 10A) to give a 6c-NO heme. The photodissociation of NO is identified by the intense instantaneous bleaching at 416 nm, accompanied by a broad induced absorption band centered at 385 nm (Fig. 10B) characteristic of a ferric 5-coordinate heme.[68] On the other side, only a largely spread absorption with very low intensity appeared, in contrast to ferrous Cyt *c*. The *time* × *wavelength* matrix of induced absorptions analyzed by SVD yielded a main spectral SVD transient component which is conspicuously different from the equilibrium difference spectrum (Fig. 10C).

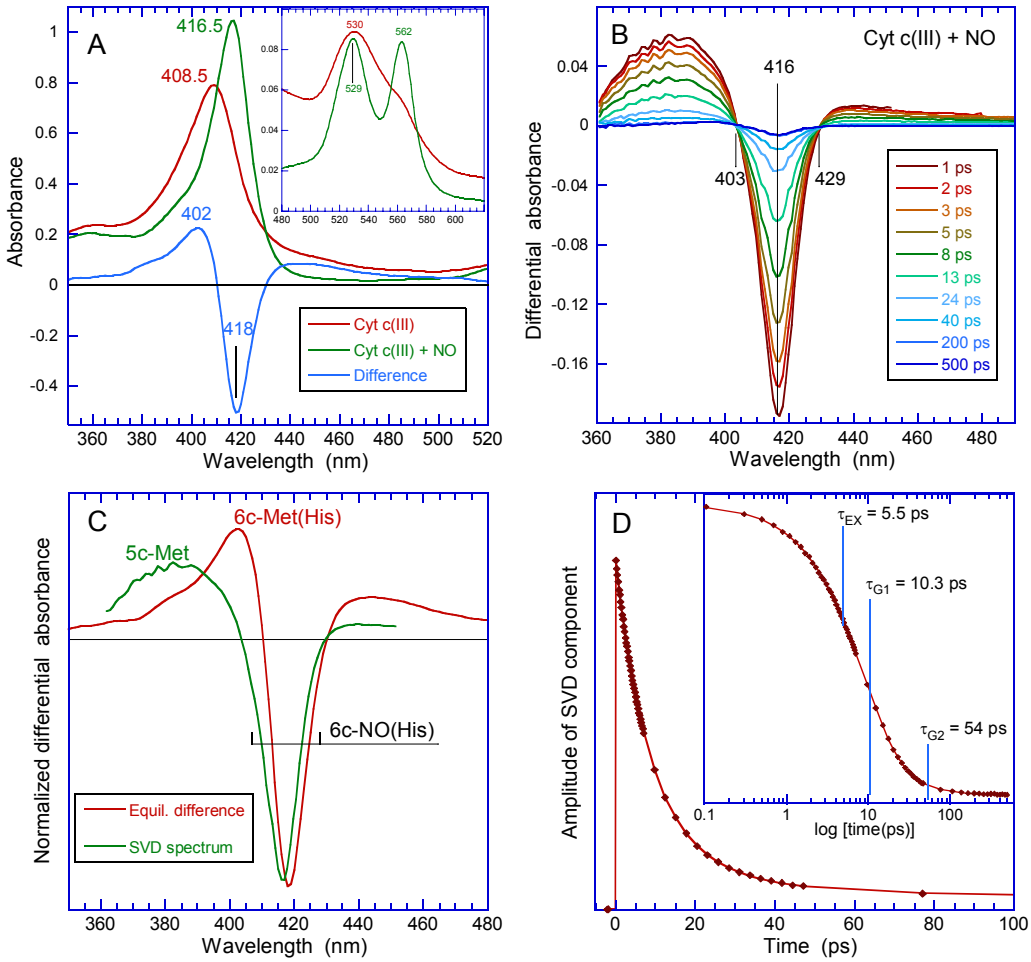


Fig. 10. (A) Equilibrium spectra of ferric Cyt *c* with and without NO. (B) Differential transient spectra of ferric Cyt *c* at various time delays after photodissociation of NO. (C) The main SVD spectral component extracted from transient data is compared with the steady-state difference. The coordination states of the heme are indicated. (D) Fitted kinetics associated with the SVD spectral component. The position of time-constants are displayed on a log scale.

The kinetics of main spectral SVD component (Fig. 10D), due to geminate NO rebinding, were fitted with a multiexponential function. The fast initial phase (τ_{ex} = 5.5 ps) corresponds to the vibrational relaxation of the heme.[31] The geminate rebinding of NO to the 5c-His ferric heme occurs in two phases having well separated time constants (τ_{G1} = 10.3 ps and τ_{G2} = 54 ps) the first one having a relative amplitude (A_1 = 88%) 10-fold larger than the second one (A_2 = 8.5%). Fitting the kinetics over the entire 500-ps range yielded a constant component (A_C = 3.5%) corresponding to the proportion of NO exiting from the heme pocket and the protein core. When probed by IR transient absorption,[69] the NO geminate rebinding was fitted with a stretched exponential function [$\exp(-(t/7\ \text{ps})^{0.7}$] which should include the second component that we measured.

Subsequent heme coordination dynamics in the nanosecond to second time range. The yield of photodissociated NO molecules that do not geminately rebind to the heme and are going out of the heme pocket was found to be very low: 1.5% for ferrous and 3.5% for ferric Cyt *c*. Therefore, studying the subsequent slower stages of heme coordination dynamics requires a different approach. Fortunately, it is possible to increase the proportion of NO molecules exiting from the heme pocket and thus to enhance the TA signal at nanosecond and longer time delays by using a 6-ns pump pulse, which induces many cycles of NO photodissociation followed by geminate rebinding, hence increasing the yield of NO release per pulse.

Ferrous Cyt c–NO. The subsequent slower dynamics of heme coordination in ferrous Cyt *c* after NO photodissociation was probed at five particular wavelengths (Fig. 11) and the transitions were identified by global analysis of the simultaneous evolution of the induced absorption and bleaching at the five wavelengths. First we note that the kinetics at 411 and 415 nm should start with a bleaching signal, according to the transient spectrum measured at 0.5 ns (Fig. 9). However all five kinetics start with a sharp decrease of the transient absorption with two successive time constants τ_1 = 6 ns and τ_2 = 0.5 μs that can neither be assigned to Met80 nor to NO geminate rebinding because of the decrease of positive amplitude at 411 and 415 nm instead of an increase from bleaching. We therefore interpret this signal as a photoreaction of the 5c His-Fe(II) heme repeatedly excited by the intense 6-ns dissociating pulse with a possible charge transfer with relaxation time constants τ_1 = 6 ns and τ_2 = 0.5 μs. This hypothesis originates from the absence of such phenomenon in the case of ferric Cyt *c* (see below). Thus, for ferrous Cyt *c*, the heme coordination dunamics was analyzed starting from ~1 μs after NO photo-dissociation.

Two transitions present the same evolution (Fig. 11): an absorbance increase at 411, 415 and 418 nm (formation of the 6c His–Fe^{2+}–Met80) with a simultaneous absorbance decrease at 425 – 430 nm (disappearance of the 5c–His–Fe^{2+}). This behavior is the signature of the Met80 rebinding which thus occurs with two phases with time constants τ_3 = 5 μs and τ_4 = 200 μs. Indeed, these transitions cannot be attributed to NO rebinding which would instead lead to a decrease at 415 and 418 nm, as observed for the slow 5-s transition, unambiguously assigned to NO bimolecular rebinding from the solution. The amplitude is veryy low at 430 nm, this wavelength being very close to the isosbestic point for Met80 rebinding. The two constants suggest the presence of two conformations for the 5c ferrous state having different energy barriers for Met80 recombination.

After the Met80 rebinding, the observed amplitude of NO bimolecular rebinding is low due to the very close Soret maxima of native (411 nm) and nitrosylated (415 nm) forms, yielding a very small absorption difference. It occurs with a time constant of 5 s in the presence of [NO] = 2.4 mM, yielding an association rate constant k_{on} = 83 $M^{-1}{\cdot}s^{-1}$. This slow association rate is due to the need for Met80 to dissociate before NO can approach the heme iron in the distal pocket and explains the accumulation of some dissociated ferrous species during the steady-state Raman measurement, even at low power.

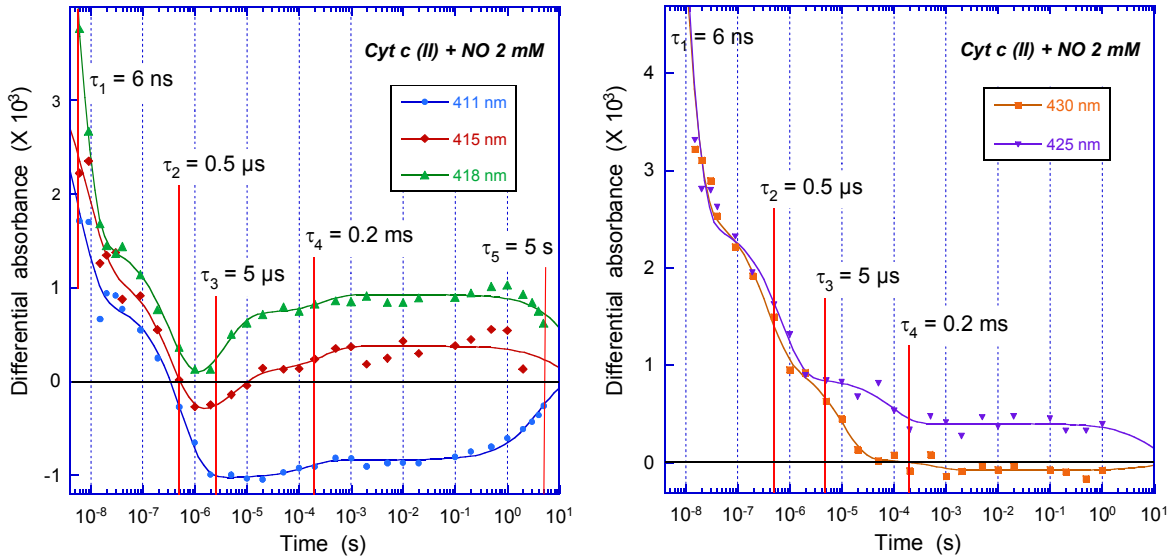


Fig. 11. Kinetics of the heme coordination in ferrous Cyt *c* after photodissociation of NO recorded at five particular wavelengths from 1 ns to 5 s with concentration [NO] = 2.4 mM. For the choice of the wavelegnths, see the differential spectrum at equilibrium in Fig. 8A. The kinetics are not normalized and the amplitude represents the differential absorption. The curves are fits to a function of five exponential components whose time constants are indicated by the red vertical lines. The transition τ_3 is not observed at 411 nm, whereas the transition τ_4 is within the noise at 430 nm.

Ferric Cyt c–NO. The TA kinetics after NO photodissociation from ferric nitrosylated Cyt *c* was similarly recorded at eight particular wavelengths (Fig. 12). The Met80 rebinding is identified by an absorbance decrease at 392 nm which corresponds to the disappearance of 5c His–Fe^{3+} (Fig. 12A), accompanied by an absorption increase at 406 – 408 nm, wavelengths close to the maximum of the Soret band of 6c His–Fe^{3+}–Met80 species (Fig. 12B). There are two such transitions, occurring with successive time constants τ_1 = 40 ns and τ_2 = 3.3 µs, the latter one having a larger amplitude. The rebinding of the distal Met80 with two different time constants again suggests the existence of two different configurations of the ferric Cyt *c*.

The bimolecular NO rebinding corresponds to a simultaneous decrease of the differential amplitude, absorption or bleaching, at all wavelengths. It is readily identified by

changing the NO concentration by a factor of 10, which shifted the observed transition by one decade, from 0.23 ms to 2.2 ms, for respectively 2.4 mM and 0.24 mM of NO (Fig. 12C and D). This yields an association rate constant k_{on} = 1.8 × 10^6 $M^{-1}{\cdot}s^{-1}$. A second transition occurred at τ_4 = 88 ms ([NO] = 2.4 mM) and ~300 ms ([NO] = 0.24 mM) with similar spectral signature, which is thus also assigned to bimolecular rebinding (the transition τ_4 does not appear shifted by a decade probably because of the loosely defined baseline after 0.3 s). Again, the presence of two transitions, both assigned to bimolecular rebinding, suggests the existence of two different conformations of ferric Cyt *c*, a hypothesis supported by the fact that after the first NO rebinding (τ_3) the differential amplitude kinetics at 407–408 nm became positive (at ~0.5 ms) implying that the two conformations of ferric Cyt *c* do not have exactly the same Soret maximum. No transitions other than Met80 and NO rebinding were identified.

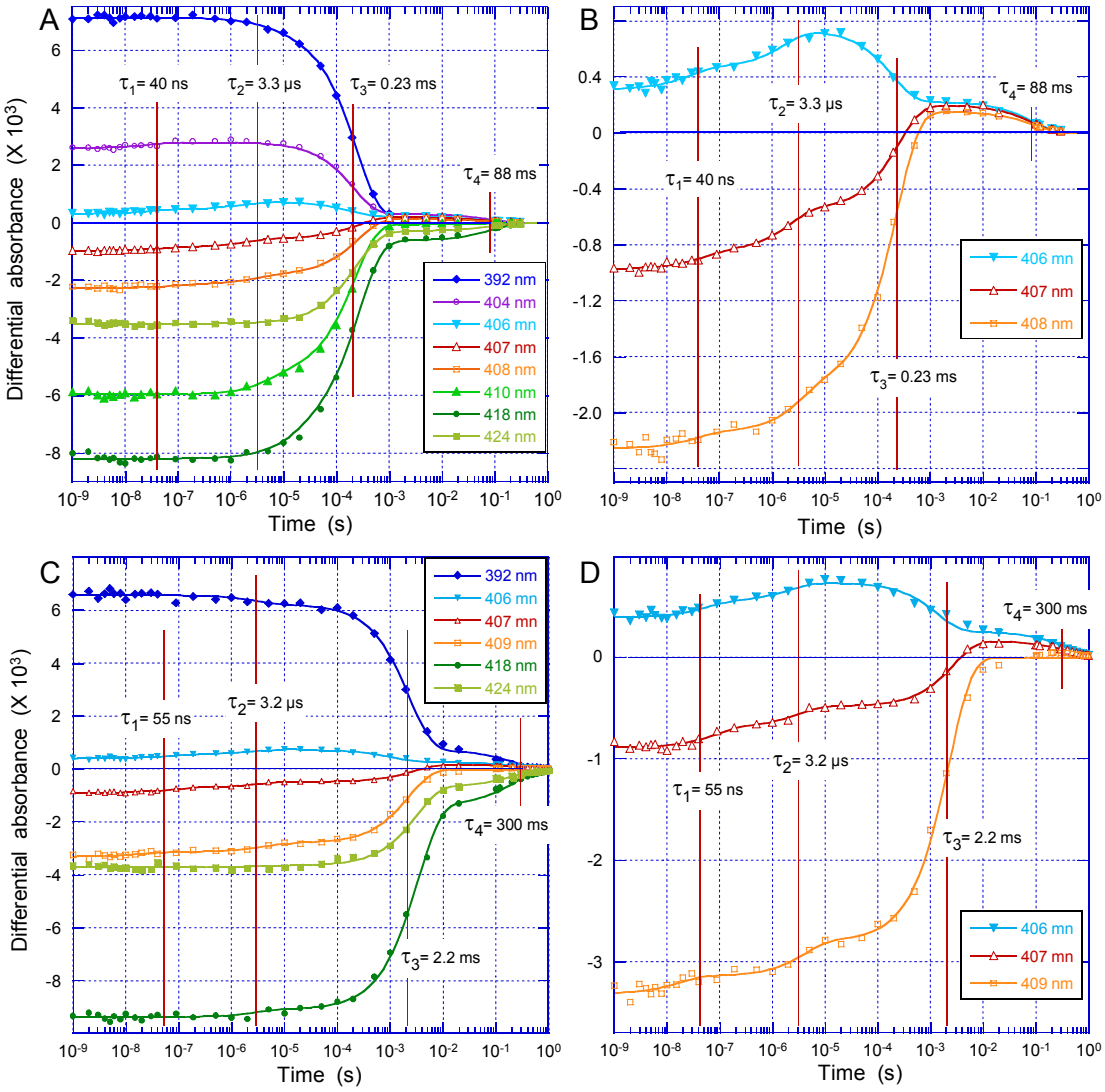


Fig. 12. Kinetics of the heme coordination in ferric Cyt *c* after photodissociation of NO recorded from 1 ns to 1 s at two different NO concentrations. (A) Kinetics at eight particular wavelengths, not normalized, for [NO] = 2.4 mM. (B) The kinetics at wavelengths close to the isobestic point of Met80 rebinding (see Fig. 7) are enlarged for [NO] = 2.4 mM. (C) Kinetics at six particular wavelengths for

[NO] = 0.24 mM. (D) Enlarged kinetics close to the isobestic point of Met80 rebinding for [NO] = 0.24 mM. The curves are fits of the data points to a function comprising four exponential components whose time constants are indicated by the red vertical lines.

These observations imply that the interconversion between both ferric Cyt *c* conformations must be slower. We cannot deduce the interconversion rate from our data. However, since the association rate k_{on} is strongly influenced, the conformations at the heme level should be markedly different between both populations, consistent with a rather high energy barrier which should favor a slow interconversion.

Dynamics of NO rebinding. The main component of NO geminate rebinding to both ferrous and ferric Cyt *c* is very fast (9.2 and 10.3 ps) with large amplitude. It is the faster rebinding measured among 5c-His heme proteins (Tables 4 and S1) being however slightly slower than that observed for NO rebinding to the 4-coordinate heme proteins (7.5 ps) whose bond between iron and the proximal His is cleaved after NO ligation.[66,70,71] In the latter case, the very fast NO back ligation is due to the high reactivity of the 4c-heme whereas for 5c-His Cyt *c* the very fast NO rebinding is due to steric factors which increase the energy barrier preventing the exit of NO from the heme pocket, most probably due to the distal methionine which did not yet rebind to the iron after 0.5 ns. Although the geminate yield is as large as that measured for 4c-hemes (98.5%) it differentiates from these proteins by the presence of two geminate components, as observed for myoglobin[72] and for the L16A mutant of the bacterial NO-carrier cytochrome *c*' from *Alcaligenes xylosoxidans*.[73] In both redox states NO geminate rebinding occurs with a second phase having same time constant (55 ps) and a small proportion of NO exiting the heme pocket (1.5 – 3.5%). Thus the second component τ_{G2} does not depend on the redox state of the heme and we assign it to a protein structural feature.

Since the transition τ_3 depends upon [NO] we calculated $k_{on} = 1.8 \times 10^6$ $M^{-1}{\cdot}s^{-1}$ for ferric Cyt *c*–NO formation, based on $\tau_3 = 0.23$ ms in the presence of 2.4 mM NO (at 20 °C). This is much larger than the estimated value (7.2×10^2 $M^{-1}{\cdot}s^{-1}$) from an early flash-photolysis study[74] which assigned the transition at 0.2 ms to a structural rearrangement rather than to NO bimolecular rebinding.[74] The ferric Cyt *c*–NO association rate thus appears of the same order of magnitude as other ferric heme proteins[75] and especially is the same as in ferric nitrophorin but ten times faster than in ferric Mb. In the presence of cardiolipin bound to the ferric Cyt *c* two bimolecular rebinding components were observed,[42] one yielding exactly the same k_{on} (1.8×10^6 $M^{-1}{\cdot}s^{-1}$) as we measured (the other component yielded 0.55×10^6 $M^{-1}{\cdot}s^{-1}$). This suggests that one of these species in the presence of cardiolipin keeps the native conformation of ferric Cyt *c*.

Table 4. Time constants and amplitudes of the transitions in the time range 1 ps – 5 s.

Transition		Ferric Cyt c 2.4 mM NO	Ferric Cyt c 0.24 mM NO	Ferrous Cyt c 2.4 mM NO
NO geminate rebinding	τ_{G1} τ_{G2} constant	–	10.3 ± 0.5 ps (88)[a] 54 ± 7 ps (8.5) (3.5)	9.2 ± 0.5 ps (92.7) 55 ± 8 ps (5.7) (1.5)
Met80 rebinding	τ_{M1}	40 ± 20 ns (30)[a]	55 ± 20 ns (40)	5 ± 1 µs (70)
	τ_{M2}	3.3 ± 0.5 µs (70)	3.2 ± 0.7 µs (60)	200 ± 100 µs (30)
NO bimolecular rebinding	τ_3	0.23 ± 0.02 ms (95)	2.2 ± 0.1 ms (85)	–
	τ_4	88 ± 20 ms (5)	300 ± 50 ms (15)	5 ± 1 s
	k_{on} (b)	1.8×10^6 $M^{-1}\cdot s^{-1}$	1.8×10^6 $M^{-1}\cdot s^{-1}$	83 $M^{-1}\cdot s^{-1}$

(a) Relative amplitudes (%) of the components. The vibrational relaxation is not included, only the heme coordination changes.
(b) For the ferric form k_{on} corresponds to the major transition τ_3, but to the unique τ measured for the ferrous form.

The faster k_{on} for ferric compared to ferrous Cyt *c* originates from the low energy of thermal breaking of the Fe–Met bond which is already broken at 59 °C,[76] (but this bond cannot be photolyzed in the ferric state,[31] and the cleavage occurrs through a different process). Contrastingly, the Fe–Met in ferrous Cyt *c* bond is stable even at 80 °C,[77] and should break only transiently at very slow rate so that it decreases the NO association rate k_{on} as low as 83 $M^{-1}\cdot s^{-1}$.

Comparison with other Heme Proteins. The interaction of NO and other diatomics with various heme proteins sensors which are 5-coordinated in native state has been rationalized using a "sliding scale rule".[78] The behavior of Cyt *c* (which does not bind CO and O_2) appears clearly determined by its 6th heme ligand Met80 and cannot be described by this rule, likewise the sensor Dos which discloses similarly low association rates ($1.1 – 2.6 \times 10^3$ $M^{-1}s^{-1}$)[79] and does not discriminate the three diatomics NO, O_2 and CO.

Dynamics of methionine rebinding. The cleavage of the Fe–Met80 bond plays a role in processes such as the cardiolipin-Cyt *c* interaction[14] and Cyt *c* release from mitochondria during apoptosis.[80] Here, we identified and separated the Met80 and NO rebinding based on their spectral signatures. The kinetics in the 1 ns – 1 s time range demonstrate that for both ferric and ferrous nitrosylated Cyt *c* the distal ligand Met80 recombines much slower than NO geminate rebinding, but much faster than NO bimolecular rebinding. Two distinct rates of Met80 recombination are observed (Table 4), revealing two conformations: the major (70%) conformation has same rate in both oxidation states (3.3 – 5 µs), whereas the minor

conformations (30%), have very different rates (40 – 55 ns and 200 μs for ferric and ferrous forms) but there is no possibility to infer their structural particularities and the features which determine the corresponding energy barriers. Remarkably, the same rate as that for the major conformation ($0.2 – 0.3 \times 10^6$ s^{-1}) was measured for Met80 rebinding during the folding of ferrous Cyt *c* induced either by photodissociation of CO (0.5×10^6 s^{-1})[81] or by reduction of the ferric form (0.4×10^6 s^{-1}).[82,83] The fact that the Met80 rebinding occurs with same time constant during folding process or after NO exiting the heme pocket suggests that the protein structure, not the redox state, governs the dynamics of Met80 and its encounter with the heme iron. In this sense, the reformation of the distal heme coordination Fe–Met80 in Cyt *c* (3 – 5 μs) plays a totally different role than reformation of the proximal Fe–His bond in the bacterial cytochrome *c*' (100 ps), which acts as a ligand trap.[70] The rate of Fe–Met bond reformation is faster than that in the O_2-sensor DOS which occurs with a 100-μs time constant,[19] but which is accompanied by a conformational change of the whole protein structure, but in Cyt *c* the structural change is limited to the heme pocket. The major part of Met80 rebinding (3 – 5 μs) is 10^6 times slower than after its photodissociation in the absence of NO (~5 ps),[31] implying that the heme pocket structural conformation has substantially changed after replacement of Met80 with NO.

We found from Raman data that the 6-coordinate His–Fe(II)–NO and His–Fe(II)–Met80 Cyt *c* species possess very different heme structural conformations with respect to ruffling distortion; this fact may explain large difference of energy barriers for Met80 recombination between the minor conformations of the two redox states.

The existence of two geminate rebinding phases is due to structural constraints on NO movement in the heme pocket, probably correlated with two conformations of Met80 in the 5c transient species after NO dissociation. In one of the conformations, Met80 rebinding has the same time constant in the ferric (τ_3 = 3.3 μs) and ferrous (τ_3 = 5 μs) redox states. Remarkably, even for native Cyt *c* after the photo-detachment of Met80 (in the absence of NO) the reformation of the Fe(II)–Met80 bond also takes place in two phases (time constants of 5 and 16 ps)[31] but much faster than after NO release (3.3 μs and 200 μs). In the native Cyt *c* these two phases probably relate to two different rotational positions of the detached Met80 side-chain,[84] which can also be the case for nitrosylated Cyt *c*.

Conclusions

All the present results demonstrate the differences of structural and dynamic properties of nitrosylated compared to native Cyt *c*, and also between the ferrous and ferric redox states. The Raman data reveal that nitrosylation of ferrous Cyt *c* increases the heme ruffling distortion, while for ferric Cyt *c*–NO the dominant ruffling distortion largely disappears, resulting in more relaxed heme structure. In ferrous Cyt *c*, the sixth distal ligand, NO or Met80, can be photodissociated whereas in ferric Cyt *c* only NO can be photodissociated and Met80 cannot. Another proof of the difference of heme conformation between the native and the nitrosylated complexes is given by the position of iron-histidine stretch in Raman spectra of ferrous transient species. The central iron is displaced much further away from the heme plane towards proximal histidine after Met80 detachment than after NO detachment which results in smaller out-of-plane iron movement. Remarkably, the methionine rebinding (3 – 5 μs) is 6 orders of magnitude slower than after its photodissociation in absence of NO (~5 ps), again meaning that the heme pocket structural conformation is substantially different after replacement of Met80 with NO.

The bimolecular binding of NO to Cyt *c* also strongly depends on the heme redox state with association rate ($k_{on}^{Fe(III)} = 1.8 \times 10^6$ $M^{-1}s^{-1}$ and $k_{on}^{Fe(II)} = 83$ $M^{-1}s^{-1}$) differing by more than 4 orders of magnitude because of a much stronger Fe–Met80 bond in the ferrous state. The unusually low $k_{on}^{Fe(II)}$ explains that ferrous Cyt *c* was often considered as not binding NO. Altogether, our data demonstrate that after disruption of Fe−Met80 bond, pronounced heme conformational changes are stabilized by the occupancy of the 6th axial position by NO, which is no longer coupled to the distal protein structure. Conformational changes are associated with physiological properties[24] of Cyt *c* and depend on redox state of the heme. The unique structural and dynamic properties of Cyt *c* in interaction with nitric oxide are relevant for its interactions with anionic lipids, with membrane, and for the molecular mechanism of apoptosis in general.

Conflict of interest

There are no conflicts of interest to declare.

Acknowledgements

The authors acknowledge the help provided by Simona Cianetti during the first stage of this work.

Dedication

This article is dedicated to the memory of Fabrice Rappaport (Laboratoire de Physiologie

Membranaire et Moléculaire du Chloroplaste, Université Pierre et Marie Curie, Paris, France) who passed away on january 12, 2016, with whom we recorded the transient absorption data in the nanosecond to second time range.

References

1 L. Banci and M. Assfalg. Handbook of metalloproteins. John Wiley Ed., Chichester, UK.: 2001; pp 33−43.

2 Y. L. P. Ow, D. R. Green, Z. Hao and T. W. Mak. *Nat. Rev. Mol. Cell Biol.*, 2008, **9**, 532−542.

3 X. S. Liu, C. N. Kim, J. Yang, R. Jemmerson and X. D. Wang. *Cell*, 1996, **86**, 147−157.

4 H. Zou, W. J. Henzel, X. S. Liu, A. Lutschg and X. D. Wang. *Cell*, 1997, **90**, 405−413.

5 H. Zou, Y. C. Li, H. S. Liu and X. D. Wang. *J. Biol. Chem.*, 1999, **274**, 11549−11556.

6 C. M. Schonhoff, B. Gaston and J. B. Mannick. *J. Biol. Chem.*, 2003, **278**, 18265−18270.

7 P. Ghafourifar, U. Schenk, S. D. Kelin and C. Richter. *J. Biol. Chem.*, 1999, **274**, 31185−31188.

8 A. Tatoyan and C. Giulivi. *J. Biol. Chem.*, 1998, **273**, 11044−11048.

9 C. Giulivi. *Free Radic. Biol. Med.*, 2003, **34**, 397−408.

10 N. J. Török, H. Higuchi, S. Bronk and G. J. Gores. *Cancer Res.*, 2002, **62**, 1648−1653.

11 H. T. Chung, H. O. Pae, B. M. Choi, T. R. Billiar and Y. M. Kim. *Biochem. Biophys. Res. Commun.*, 2001, **282**, 1075−1079.

12 B. Zech, R. Kohl, A. von Knethen and B. Brune. *Biochem. J.*, 2003, **371**, 1055−1064.

13 S. Berezhna, H. Wohlrab and P. M. Champion. *Biochemistry*, 2003, **42**, 6149−6158.

14 A. A. Kapralov, I. V. Kurnikov, I. I. Vlasova, N. A. Belikova, V. A. Tyurin, L. V. Basova, Q. Zhao, Y. Y. Tyurina, J. Jiang, H. Bayir, Y. A. Vladimirov and V. E. Kagan. *Biochemistry*, 2007, **46**, 14232−14244.

15 L. V. Basova, I. V. Kurnikov, L. Wang, V. B. Ritov, N. A. Belikova, I. I. Vlasova, A. A. Pacheco, D. E. Winnica, J. Peterson, H. Bayir, D. H. Waldeck and V. E. Kagan. *Biochemistry*, 2007, **46**, 3423−3434.

16 R. Jemmerson, J. Liu, D. Hausauer, K. P. Lam, A. Mondino and R. D. Nelson. *Biochemistry*, 1999, **38**, 3599−3609.

17 P. J. R. Spooner and A. Watts. *Biochemistry*, 1992, **31**, 10129−10138.

18 S. S. Paul, P. Sil, S. Haldar, S. Mitra and K. Chattopadhyay. *J. Biol. Chem.*, 2015, **290**, 14476−14490.

19 U. Liebl, L. Bouzhir-Sima, L. Kiger, M. C. Marden, J.-C. Lambry, M. Negrerie and M. H. Vos. *Biochemistry*, 2003, **42**, 6527−6535.

20 N. Osheroff, D. Borden, W. H. Koppenol and E. Margoliash. *J. Biol. Chem.*, 1980, **255**, 1689−1697.

21 P. Ascenzi, M. Coletta, R. Santucci, F. Polizio and A. Desideri. *J. Inorg. Biochem.*, 1994, **53**, 273−280.

22 M. A. Sharpe and C. E. Cooper. *Biochem. J.*, 1998, **332**, 9−19.

23 S. Basu, N. A. Azarova, M. D. Font, S. B. King, N. Hogg, M. T. Gladwin, S. Shiva and D. B. Kim-Shapiro. *J. Biol. Chem.*, 2008, **283**, 32590−32597.

24 L. Hannibal, F. Tomasina, D. A. Capdevila, V. Demicheli, V. Tortora, D. Alvarez-Paggi, R. Jemmerson, D. H. Murgida and R. Radi. *Biochemitry*, 2016, **55**, 407−428.

25 M. T. de Groot, M. Merkx and M. T. M. Koper. *Langmuir*, 2007, **23**, 3832−3839.

26 G. Battistuzzi, M. Borsari, J. A. Cowan, A. Ranieri and M. Sola. *J. Am. Chem. Soc.*, 2002, **124**, 5315−5324.

27 I. I. Vlasova, V. A. Tyurin, A. A. Kapralov, I. V. Kurnikov, A. N. Osipov, M. V. Potapovich, D. A. Stoyanovsky and V. E. Kagan. *J. Biol. Chem.*, 2006, **281**, 14554−14562.
28 P. X. R. Qi, R. A. Beckman and A. J. Wand. *Biochemistry*, 1996, **35**, 12275−12286.
29 S. G. Kruglik, J. C. Lambry, J. L. Martin, M. H. Vos and M. Negrerie. *J. Raman Spectrosc.*, 2011, **42**, 265−275.
30 G. Hui-Bon-Hoa, H. Kaddour, J. Vergne, S. G. Kruglik and M. C. Maurel. *BMC Biophysics*, 2014, **7**, 2.
31 M. Negrerie, S. Cianetti, M. H. Vos, J. L. Martin and S. G. Kruglik. *J. Phys. Chem. B*, 2006, **110**, 12766−12781.
32 K. D. Vandegriff and R. I. Shrager. *Methods Enzymol.*, 1994, **232**, 460−485.
33 D. Beal, F. Rappaport and P. Joliot. *Rev. Sci. Instrum.*, 1999, **70**, 202−207.
34 S. Hu, I. K. Morris, J. P. Singh, K. M. Smith and T. G. Spiro. *J. Am. Chem. Soc.*, 1993, **115**, 12446−12458.
35 Y. H. Sun, A. Benabbas, W. Q. Zeng, J. G. Kleingardner, K. L. Bren and P. M. Champion. *Proc. Natl. Acad. Sci. U.S.A.*, 2014, **111**, 6570−6575.
36 E. Santoni, S. Scatragli, F. Sinibaldi, L. Fiorucci, R. Santucci and G. Smulevich. *J. Inorg. Biochem.*, 2004, **98**, 1067−1077.
37 S. S. Stavrov. *Biophys. J.*, 1993, **65**, 1942−1950.
38 P. M. Champion, B. R. Stallard, G. C. Wagner and I. C. Gunsalus. *J. Am. Chem. Soc.*, 1982, **104**, 5469−5472.
39 O. Bangcharoenpaurpong, P. M. Champion, K. S. Hall and L. P. Hager. *Biochemistry*, 1986, **25**, 2374−2378.
40 J. A. Shelnutt, X. Z. Song, J. G. Ma, S. L. Jia, W. Jentzen and C. Medforth. *Chem. Soc. Rev.*, 1998, **27**, 31−41.
41 C. Olea, J. Kuriyan and M. A. Marletta. *J. Am. Chem. Soc.*, 2010, **132**, 12794−12795.
42 G. Silkstone, S. M. Kapetanaki, I. Husu, M. H. Vos and M. T. Wilson. *Biochemistry*, 2012, **51**, 6760−6766.
43 K. Prendergast and T. G. Spiro. *J. Am. Chem. Soc.*, 1992, **114**, 3793−3801.
44 V. Karunakaran, Y. Sun, A. Benabbas and P. M. Champion. *J. Phys. Chem. B.*, 2014, **118**, 6062−6070.
45 A. M. Berghuis and G. D. Brayer. *J. Mol. Biol.*, 1992, **223**, 959−976.
46 G. Smulevich, M. J. Bjerrum, H. B. Gray and T. G. Spiro. *Inorg. Chem.*, 1994, **33**, 4629−4634.
47 M. N. Siamwiza, R. C. Lord, M. C. Chen, T. Takamatsu, I. Harada, H. Matsuura and T. Shimanouchi. *Biochemistry*, 1975, **14**, 4870−4876.
48 B. Hernandez, Y.-M. Coïc, F. Pflüger, S. G. Kruglik and M. Ghomi. *J. Raman Spectrosc.*, 2016, **47**, 210−220.
49 D. Aslanian, T. Heidmann, M. Negrerie and J. P. Changeux. *FEBS Letters*, 1983, **164**, 393−400.
50 J. Kim, J. Park, T. Lee and M. Lim. *J. Phys. Chem. B*, 2012, **116**, 13663−13671.
51 T. Takano and R. E. Dickerson. *Proc. Natl. Acad. Sci. U.S.A.*, 1980, **77**, 6371−6375.
52 B. Benko and N.-T. Yu. *Proc. Natl. Acad. Sci. U.S.A.*, 1983, **80**, 7042−7046.
53 A. Almohammedi, S. M. Kapetanaki, A. J. Hudson and N. M. Storey. *Anal. Chem.*, 2015, **87**, 10605−10612.
54 T. G. Spiro and X. Y. Li. *Biological Applications of Raman Spectroscopy*. John Wiley & Sons, Inc., New York.: 1988; Vol. 3, p 1−37.
55 A. P. Hunt and N. Lehnert. *Accounts Chem. Res.*, 2015, **48**, 2117−2125.

56 T. Tomita, N. Haruta, M. Aki, T. Kitagawa and M. Ikeda-Seito. *J. Am. Chem. Soc.*, 2001, **123**, 2666−2667.

57 M. M. Maricq, N. A. Tanguay, J. C. O'Brien, S. M. Rodday and E. Rinden. *J. Chem. Phys.*, 1989, **90**, 3136−3144.

58 V. K. K. Praneeth, F. Paulat, T. C. Berto, S. DeBeer-George, C. Näther, C. D. Sulok and N. Lehnert. *J. Am. Chem. Soc.*, 2008, **130**, 15288−15303.

59 G. V. Louie and G. D. Brayer. *J. Mol. Biol.*, 1990, **214**, 527−555.

60 S. G. Kruglik, B. K. Yoo, S. Franzen, M. H. Vos, J. L. Martin and M. Negrerie. *Proc. Natl. Acad. Sci. U.S.A.*, 2010, **107**, 13678−13683.

61 B. K. Yoo, S. G. Kruglik, I. Lamarre, J. L. Martin and M. Negrerie. *J. Phys.Chem. B*, 2012, **116**, 4106−4114.

62 S. Othman, A. Lelirzin and A. Desbois. *Biochemistry*, 1993, **32**, 9781−9791.

63 T. Kitagawa. The heme protein structure and the iron histidine stretching mode. In *Biological applications of Raman spectroscopy*, Spiro, T., Ed. Wiley: New-York, 1988; Vol. 3, p 97−131.

64 S. Cianetti, M. Negrerie, M. H. Vos, J. L. Martin and S. G. Kruglik. *J. Am. Chem. Soc.*, 2004, **126**, 13932−13933.

65 J. P. M. Schelvis, S. Kim, Y. Zhao, M. A. Marletta and G. T. Babcock. *J. Am. Chem. Soc.*, 1999, **121**, 7397−7400.

66 B. K. Yoo, I. Lamarre, J. L. Martin and M. Negrerie. *J. Biol. Chem.*, 2012, **287**, 6851−6859.

67 S. Kim, G. Jin and M. Lim. *J. Phys. Chem. B*, 2004, **108**, 20366−20375.

68 C. Ramos-Alvarez, B. K. Yoo, R. Pietri, I. Lamarre, J. L. Martin, J. Lopez-Garriga and M. Negrerie. *Biochemistry*, 2013, **52**, 7007−7021.

69 J. Park, T. Lee and M. Lim. *J. Phys. Chem. B*, 2013, **117**, 12039−12050.

70 B. K. Yoo, I. Lamarre, J. L. Martin, C. R. Andrew and M. Negrerie. *J. Am. Chem. Soc.*, 2013, **135**, 3248−3254.

71 A. Benabbas, X. Ye, M. Kubo, Z. Y. Zhang, E. M. Maes, W. R. Montfort and P. M. Champion. *J. Am. Chem. Soc.*, 2010, **132**, 2811−2820.

72 B. K. Yoo, I. Lamarre, J. L. Martin, F. Rappaport and M. Negrerie. *Proc. Natl. Acad. Sci. U.S.A.*, 2015, **112**, E1697−E1704.

73 C. R. Andrew, O. N. Petrova, I. Lamarre, J.-C. Lambry, F. Rappaport and M. Negrerie. *ACS Chem. Biol.*, 2016, **11**, 3191−3201.

74 M. Hoshino, K. Ozawa, H. Seki and P. C. Ford. *J. Am. Chem. Soc.*, 1993, **115**, 9568−9575.

75 P. C. Ford and I. M. Lorkovic. *Chem. Rev.*, 2002, **102**, 993−1017.

76 G. Taler, A. Schejter, G. Navon, I. Vig and E. Margoliash. *Biochemistry*, 1995, **34**, 14209−14212.

77 R. Varhac, M. Antalik and M. Bano. *J. Biol. Inorg. Chem.*, 2004, **9**, 12−22.

78 A. L. Tsai, V. Berka, E. Martin and J. S. Olson. *Biochemistry*, 2011, **51**, 172−186.

79 G. Gonzales, E. M. Dioum, C. M. Bertolucci, T. Tomita, M. Ikeda-Saito, M. R. Chessman, N. J. Watmough and M. A. Gilles-Gonzales. *Biochemistry*, 2002, **41**, 8414−8421.

80 L. C. Godoy, C. Munoz-Pinedo, L. Castro, S. Cardaci, C. M. Schonhoff, M. King, V. Tortora, M. Marin, Q. Miao, J. F. Jiang, A. Kapralov, R. Jemmerson, G. G. Silkstone, J. N. Patel, J. E. Evans, M. T. Wilson, D. R. Green, V. E. Kagan, R. Radi and J. B. Mannick. *Proc. Natl. Acad. Sci. U.S.A.*, 2009, **106**, 2653−2658.

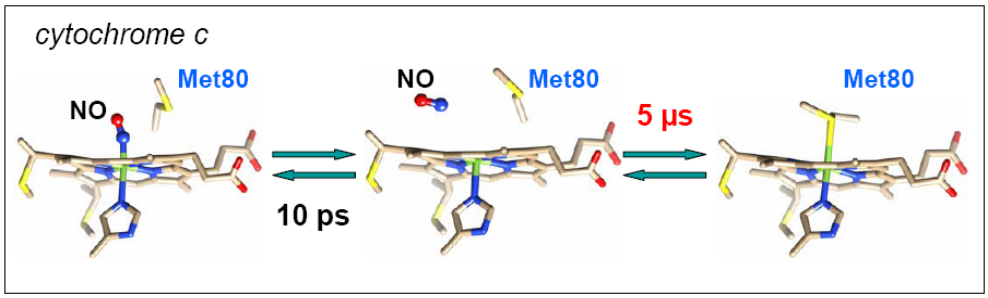
81 E. F. Chen, M. J. Wood, A. L. Fink and D. S. Kliger. *Biochemistry*, 1998, **37**, 5589−5598.

82 J. Choi, M. Fujitsuka, S. Tojo and T. Majima. *J. Am. Chem. Soc.*, 2012, **134**, 13430−13435.

83 J. Choi, D. W. Cho, S. Tojo, M. Fujitsuka and T. Majima. *Mol. Biosyst.*, 2015, **11**, 218−222.

84 P. Zhang, E. Małolepsza and J. E. Straub. *J. Phys. Chem. B*, 2012, **116**, 6980−6990.

Graphic for on-line table of content:



Structural changes and picosecond to second dynamics of cytochrome *c* in interaction with nitric oxide in ferrous and ferric redox states

Sergei G. Kruglik[1], Byung-Kuk Yoo[2], Jean-Christophe Lambry[2], Jean-Louis Martin[2] and Michel Negrerie[2,*]

[1]Laboratoire Jean Perrin, CNRS, UPMC Université Paris 6, Sorbonne Universités, 75005 Paris, France.

[2]Laboratoire d'Optique et Biosciences, INSERM, Ecole Polytechnique, 91128 Palaiseau, France.

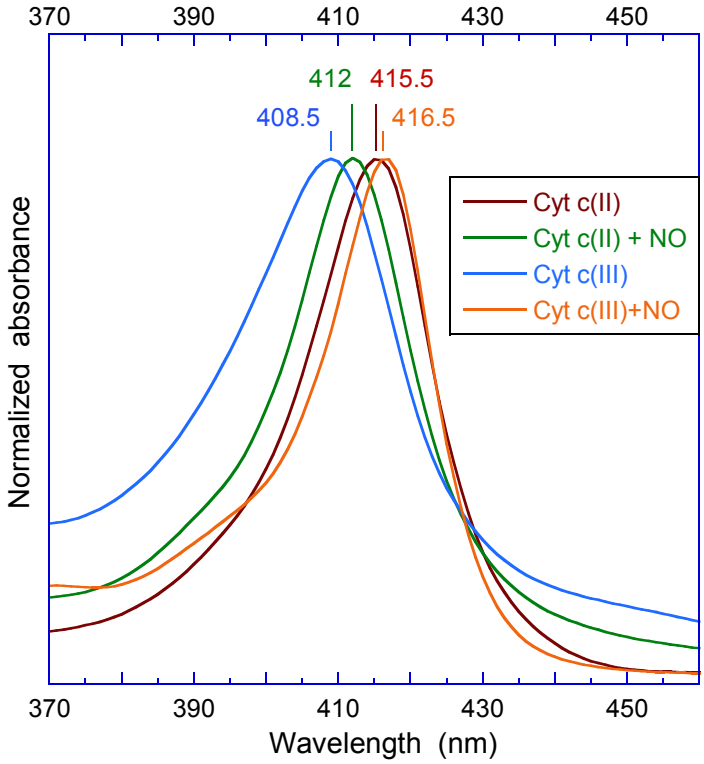


Figure S1. comparison of the Soret bands of the ferric and ferrous states of native and nitrosylated Cyt c.

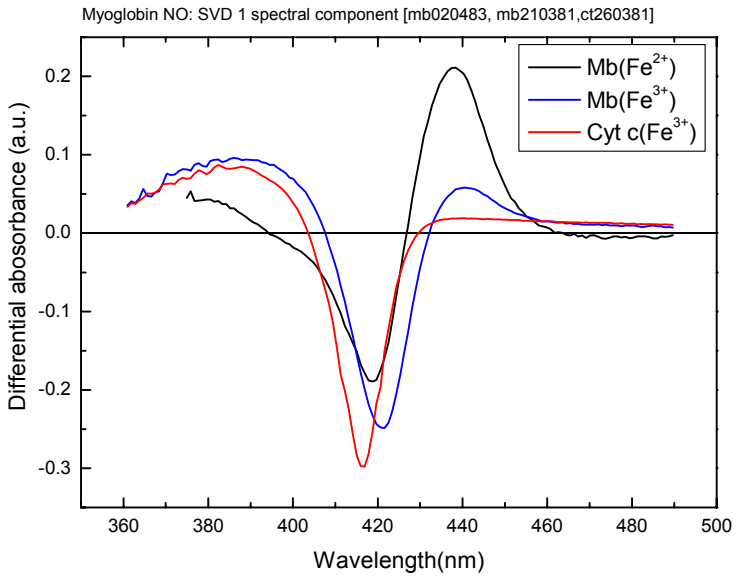


Figure S2. Comparison of the transient spectra of ferrous and ferric myoglobin with that of ferric Cyt *c* after the photodissociation of NO.

Table S1. Time constants and relative amplitudes of NO geminate rebinding of NO for various proteins which are 6-coordinate in their nitrosylated state.

Protein	**NO geminate rebinding phases**		**Constant**
	τ_{gem1} (A_1)[a]	τ_{gem2} (A_2)[a]	A_3
Fe^{2+} Cyt *c*	9.2 ps (*92.7*)	55 ps (*5.7*)	*1.5*
Fe^{3+} Cyt *c*	10.3 ps (*88*)	54.4 ps (*8.5*)	*3.5*
Lp-HbI (b)	8.0 ps (*36*)	90 ps (*62*)	*2*
Lp-HbII/III (b)	11 ps (*83*)	61 ps (*15*)	*2*
Fe^{2+} Myoglobin (c)	13 ps (*40*)	148 ps (*50*)	*10*
Fe^{3+} Myoglobin (c)	24 ps (*14*)	208 ps (*48*)	*38*
Hemoglobin (c)	10.8 ps (*74*)	61 ps (*22*)	*4*
Dehaloperoxidase (c)	14 ps (*61*)	65 ps (*38*)	*1*

(a) The amplitudes are expressed as % of the normalized transient absorption (calculated without the contributions of vibrational relaxation). All proteins are in the ferrous state except when indicated. Lp-HbI: type I hemoglobin from the invertabrate *Lucina pectinata*. Data from:
(b) Ramos-Alvarez, C.; Yoo, B.-K.; Pietri, R.; Lamarre, I.; Martin, J.-L.; Lopez-Garriga, J.; Negrerie, M. *Biochemistry* **2013**, *52*, 7007–7021.
(c) Kruglik, S. G.; Yoo, B.-K.; Franzen, S.; Vos, M. H.; Martin, J.-L.; Negrerie, M. *Proc. Natl. Acad. Sci. USA*. **2010**, *107*, 13678–13783.